Quantum dots and core shell nanoparticles of ZnS/ ZnO - Synthesis and Optical properties

A dissertation submitted in partial fulfillment of the requirement for the award of the degree of

Master of Technology
(Nanoscience and Technology)

by

SIMMI SHARMA
2K09/NST/11

Under the supervision of

Dr. Santa Chawla
Scientist 'F'
Luminescent Materials Group
Materials Physics & Engineering Division

National Physical Laboratory
Dr. K. S. Krishnan Marg, New Delhi-110012, India

Submitted to

Delhi Technological University

Formerly Delhi College of Engineering
Main Bawana Road, Shahabad, Daulatpur, Delhi-110042

June 2011

Acknowledgments

Any attempt at any level can't be satisfactorily completed without the support and guidance of learned people equally pleasant facet is to thank the people associated with the success.

First and foremost I want to express me deep sense of gratitude towards my Project Supervisor Dr. Santa Chawla ,Scientist 'F', National Physical Laboratory for her constant encouragement, constructive criticisms and full support, from the preliminary to the concluding level, despite of my stupid and irresponsible acts.

I would like to thank Professor R.K Sinha, Head, Department of Applied Physics, Delhi technological University for enabling us to carry out the project in this esteemed Laboratory, rendering help and support.

I am extremely thankful to Dr. Virender Shankar, Head of LMD group, NPL New Delhi for his constant and sincere inspiration, his liberal co-operation which really helped in the process of completion of the project.

It's my pleasure to give my sincere thanks to Dr. Harish Chander and Dr. Divi Harnath for their valuable guidance and scientific advice which helped me throughout my project work.

I express my thanks to Mrs. Jayanthi Rajan, Mrs. Sonal Sahai, Mr. Raj Kumar, Ms Shweta Sharma and Ms. Prachi Joshi for their helping nature, kind co-operation & discussions. I am also grateful to Mr. Rajgir Rai for his support and assistance from time to time.

No words can express my thanks to Mr. Atif Faiz Khan, Mr. Ravi Shanker Yadav and Mr. Abhay Deshmukh for their timely co-operation, constant help, moral support & encouragement.

I would like to thank Dr. A.K. Srivastav for doing HRTEM images of the samples and helping me understand them.

I would also like to thank Dr. R.K Kotnala & his group for their timely assistance & providing magnetic measurements.

I am thankful to Dr. Awana, Mr. Shiv Kumar, Mr Jagdish of XRD division and SEM section for helping me in Characterization of the samples.

I express my thanks to Dr. R.C. Budhani, Director, NPL and Dr. Rajeev Chopra , Scientist 'F' & Head, HRD Group, and Mr. Dharamvir Singh Saini, Technical Officer, HRD Group, NPL, for allowing me to do my M.Tech. Research Project at National Physical Laboratory.

I am thankful to Mr. K.N. Sood, Mr. Jai S. for providing SEM images of my samples.

I would like to thank all my M.Tech classmates for being always there in my hour of need.

With immense pleasure, I would like to thank all my friends Nidhi, Rashmi,Mansi, Savi, Neha for their constant care and support

At last but not least I express my love to my family members for they always stood by me and brought me to this stage. I would like to thank Almighty for having blessed me with so many loving and caring people in my life and also for constantly giving me opportunity to build my career.

(Simmi Sharma)

Certificate

This is to Certify that this dissertation entitled "**Quantum dots and core shell nanoparticles of ZnS/ ZnO - Synthesis and Optical properties"** is the bonafide work carried out by **Simmi Sharma** (2K09/NST/11) under the guidance and supervision of Dr. Santa Chawla in NPL, New Delhi-110012 and no part of this dissertation has been submitted for any other degree.

The assistance and help received during the course of investigation have been fully acknowledged.

Dr. Santa Chawla
Scientist 'F'
Luminescent Materials group
NPL, New Delhi

Dr. Rajeev Chopra
Scientist 'F'
Head, HRD
NPL, New Delhi

Date

Examiner

Place

Abstract

Quantum Dots (QD) of semiconductors could provide confinement of charge carriers in all the three dimensions and their electronic and optical properties are size dependent. Due to high surface to volume ratio, surface charges on QDs play a detrimental role in luminescence properties. With the formation of different type of core shell structure such as lower band gap core/higher band gap shell (e.g., ZnO core/ZnS shell) or inverted core/shell (e.g., ZnS core/ZnO shell) different possibilities of band structure modification and charge carrier confinement can be tailored. These structures exhibits different properties depending upon the band alignment of the core and shell semiconductor particles and hence contribute differently towards optical properties. Doping also plays a crucial role for introducing definite physical properties in quantum dots and core shell nanoparticles.

This dissertation reports the synthesis of ZnS Quantum Dots, ZnS/ZnO Inverted core shell structure and also ZnO/ZnS core shell structure. XRD and High resolution electron microscopy images unequivocally establish the formation of core shell structure. Quantum confinement effect has been observed in optical absorption and photoluminescence properties. Enhancement of ZnO excitonic emission in core shell structure and fast decay due to excitonic recombination has been observed. Effect of doping core QDs and/or shell material with magnetic impurity Chromium has been studied at room temperature and below. Doping changes the magnetic property of both ZnO and ZnS from diamagnetic to paramagnetic with enhancement of magnetization at lower temperature.

Table of Contents

Chapter1 Introduction

1.1 Quantum Dots

When an electron in a semiconductor is promoted from the valance band to the conduction band through excitation, a hole in the valance band is created. This positive hole will form a bound state with the excited negative electron by Coulomb interaction. Such bound electron hole pair is often referred to as an exciton. The spatial occupation of an exciton can be expressed in terms of an exciton Bohr radius (a_b):

$$a_b = \frac{4\pi\varepsilon_0\varepsilon_\infty \eta^2}{m_0 e^2}\left(\frac{1}{m_e^*}+\frac{1}{m_h^*}\right)$$

Where ε_∞ is the high frequency relative dielectric constant of the medium,

m_e* and m_h* are the effective masses of the electron

e is electron charge

ε_0 the vacuum permittivity

$\hbar$ represents the Planck constant.

When the particle size approaches that of the exciton Bohr radius, the exciton wave function becomes confined by the spatial limitations of the crystal. The potential barrier at the crystal surface forces the exciton wave function to go to zero at the crystal surface, confining the exciton wave function in the crystal resulting in an increase in exciton energy with decreasing crystal size, corresponding to a blue shift in both exciton absorbance and emission. Quantum Dots are semiconductor nanoparticles whose excitons are confined in all the three spatial dimension. The size related optical and electronic phenomena are also known as “quantum size effect”.

Bulk Semiconductors show a low density of states at the band edges and a quasi-continuum in band structure above and below the band gap. Density of states for a quantum well on the other hand shows a staircase type of behaviour. As consequence of the limited number of

atoms in a Quantum Dot (100-10000) the density of states shows a molecular to atomic like behaviour at the band edges as shown in fig (1.1). The discrete energy levels observed at the band edges become more pronounced with decreasing particle size as the separation between the levels increases. The ability to tune the size of quantum dots is advantageous for many applications. They are particularly significant for optical applications due to their high extinction co-efficient [1]. In electronic applications they have been proven to operate like a single-electron transistor and show the Coulomb blockade effect.

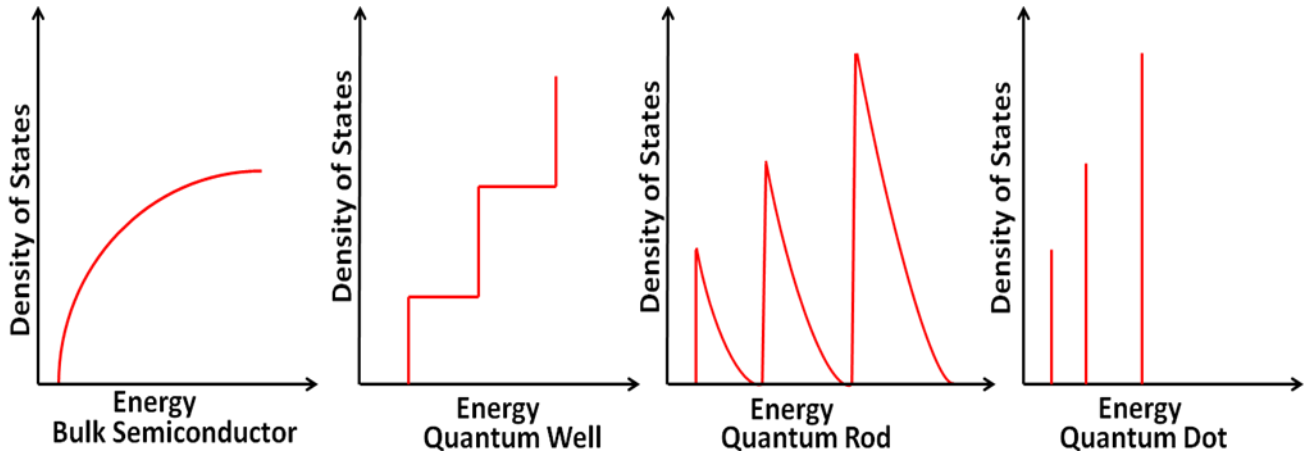

Fig.1.1 Density of states in 3D, 2D, 1D and 0D semiconductors.

Being zero dimensional, quantum dots have a sharper density of states than higher-dimensional structures. As a result, they have superior transport and optical properties, and are being researched for use in diode lasers, amplifiers, and biological sensors. Quantum dots may be excited within the locally enhanced electromagnetic field produced by the gold nanoparticles, which can then be observed from the surface Plasmon resonance in the photoluminescent excitation spectrum of nanocrystals. High-quality quantum dots are well suited for optical encoding and multiplexing applications due to their broad excitation profiles and narrow/symmetric emission spectra. The new generations of quantum dots have far-reaching potential for the study of intracellular processes at the single-molecule level, high-resolution cellular imaging, long-term in vivo observation of cell trafficking, tumour targeting, and diagnostics

Surface defects of the nanocrystal structure can cause some temporary “traps” for the electron or the hole which can affect the natural radiation recombination and become the main reason of the intermittent fluorescence (blinking). To avoid this kind of problem, we also need the shell to protect the core atoms from oxidation and other chemical reactions. To gain a large

quantum yield, we should choose the atom layers with large energy gap. And after this kind of modification, we can obtain the quantum yields close to 90%. In addition, it also enhances the photostability at the same time.

1.2 Luminescence

The term "luminescence" (Lucifer in Greek, meaning light bearer) was introduced by Eilhardt Wiedemann in 1888, in order to distinguish between light emission from thermally excited substances and light emission from molecules that have been excited by other means without increasing their average kinetic energy. Emission having an intensity that exceeds emission of the same frequency from a black body at the same temperature was termed luminescence by Wiedemann. In other words, Wiedemann characterized luminescence by the fact that it does not obey Kirchoff's law of thermal emission and absorption from a black body [2].

Types of Luminescence

Depending on excitation source of the phosphor, several types of luminescence processes are classified some are depicted in the schematic given below

Figure 1.2 Schematic Diagram Showing types of Luminescence depending upon the source of excitation

1.2.1Photoluminescence

Luminescence where the source of excitation is electromagnetic radiation is known as Photoluminescence.

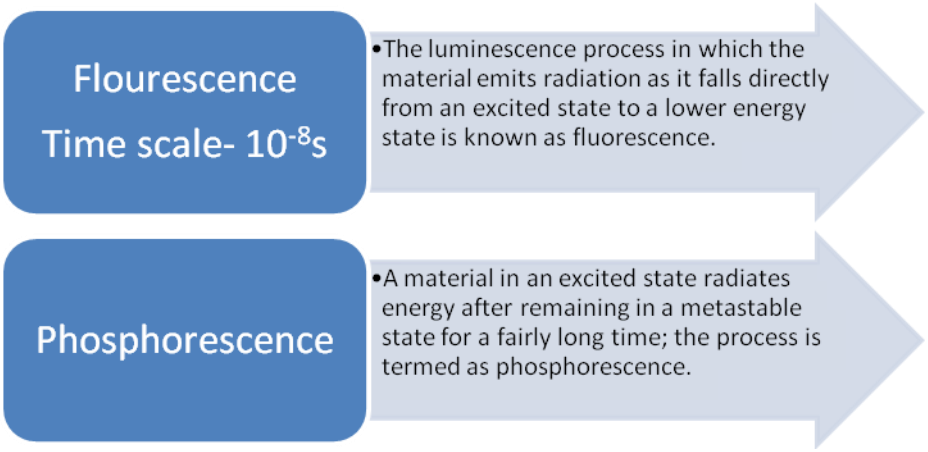

Fluorescence radiation is due to allowed transitions (S = 0) from singlet excited state to the singlet ground state. If a molecule in an excited state radiates energy after remaining in a metastable state for a fairly long time, the process is termed as phosphorescence. The time scale of the phosphorescence process depends on the recombination process between the metastable state and the nearest energy state to which transition is allowed and may be of the order of 10^{-6} second to minutes, hours or even days. This type of transition is due to forbidden transition ($S \neq 0$) from the excited metastable state to the lower ground state.

Fluorescence and Phosphorescence

The absorption of energy by a molecule raises it to an excited state. This excited state may be rotational, vibrational or electronic, depending upon the energy of exciting photon. If the energy of the exciting photon is of the order of 10^{-3} eV the rotational states can be excited, if the energy is of the order of 0.1eV then vibrational states can be excited, and if the energy is of the order of several electron volts then electronic states can be excited. The corresponding spectra are in microwave for rotational, infrared for vibrational and visible as well as ultraviolet range for electronic energy states. A molecule in an excited electronic state can loose energy and return to its ground state in a number of ways. The molecule may come to the ground state by the emission of a photon of same energy in a single step. Another possibility is, that it may loose some of its vibrational energy in collision with other molecules. Therefore downward radiative transition originates from a lower vibrational level in the upper electronic state. This phenomenon is called fluorescence and the fluorescent radiation is always of lower frequency. In molecular spectra, radiative transitions between electronic states of different total spin are prohibited (spin selection rule S = 0). Fig. 1.3 shows a situation in which a molecule in its singlet (total spin quantum no. S = 0) ground state, absorbs a photon and is raised to singlet excited state. In collisions the molecule can undergo radiationless transitions to a lower vibrational level. Now, lower vibrational level may have the same energy as one of the triplet (S = 1) excited state. There is then a certain probability of the molecule for a shift to occur to a triplet state. Further collisions in the triplet state bring the molecule's energy below that of the crossover point, so that it is now trapped in the triplet state and ultimately reaches v = 0 level.

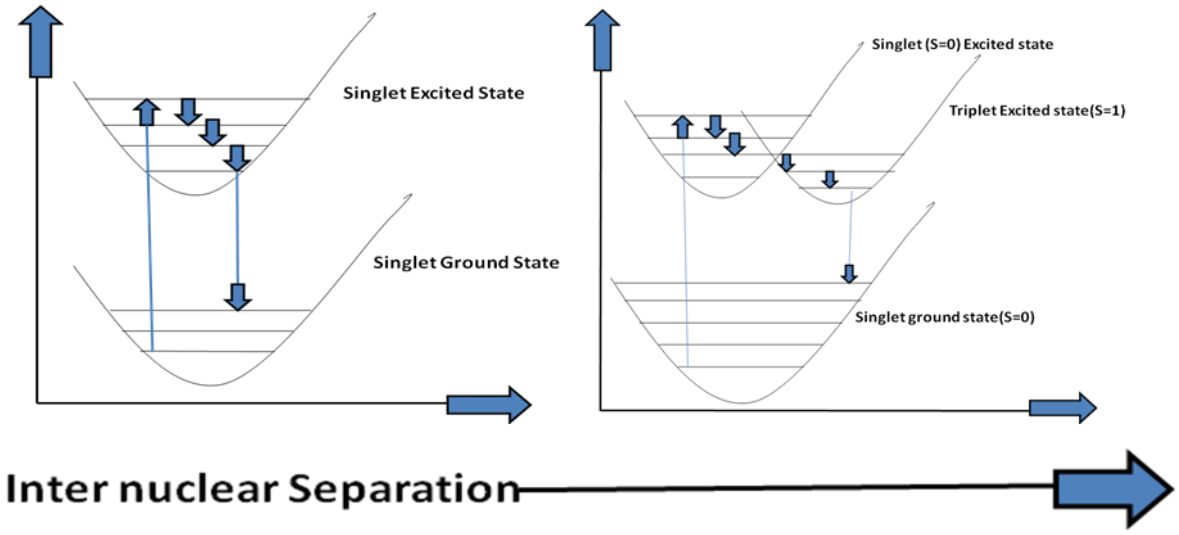

(a) Fluorescence **(b) Phosphorescence**

Fig. 1.3 graphical representation of the process of fluorescence and phosphorescence

As the radiative transition from a triplet to a singlet state is forbidden ($S \neq 1$) by spin selection rule, which means not that it is impossible but that it has only a small likelihood of occurring. Such transitions have long lifetimes, and the resulting phosphorescent radiation may be emitted in the time interval of the order of seconds, minutes or even hours after the initial excitation is switched off. Materials that show phosphorescence are known as phosphors. As our focus of study is on quantum dot that is nano dimensional we will talk about nanophosphors.

1.3 Nanophosphor

1.3.1 Theory

As discussed earlier Phosphors are Materials that convert absorbed energy to visible light without going to high temperatures i.e. incandescence. Phosphors are generally in crystalline powder form with size ranging from 1-100 µm. Phosphors with one dimension <100 nm are called nanophosphors. They possess different absorption and emission characteristics with expected improved efficiency and shorter life times that can be attributed to Quantum size effect and discrete energy levels as discussed in 1.1. As band gap can be tuned by changing the particle size, phosphors can be designed according to the device requirement. The absorption and emission spectra of nanophosphors show a blue shift because of the change in band gap energy with the particle size. The increase of the band gap with decreasing size caused by the confinement of an exciton in a finite sized crystal can be described using the "particle in a box" model. A solution for this model is presented by Brus equation given below for a spherical particle:

$$E = E_g + \frac{\eta^2 \pi^2}{2m_0 R^2}\left(\frac{1}{m_e^*} + \frac{1}{m_h^*}\right) - 1.786\frac{e^2}{4\pi\varepsilon_0\varepsilon_\infty R} + smaller \quad terms$$

The term E_g is the bulk semiconductor band gap, the second term is the solution of the Schrödinger equation for a particle in a spherical potential well, with a $1/R^2$ dependence where R represents the crystal radius. The third term describes the decrease in energy as result of the free electron and hole Coulomb attraction. A second effect which is observed as result of the decrease in crystal size is the appearance of discrete energy levels at the band edges.

1.3.2 Application of Nanophosphors

Nanophosphors have applications in displays like television i.e. cathode ray tubes (CRT), plasma display panels (PDP), Electroluminescence (EL) based displays and field emission displays; in light sources like fluorescent tubes, compact fluorescent lamps and cold cathode lamps; as detectors for x-rays, temperature and pressure. Up-converting and down converting phosphors in nanosizes have great promise in increasing efficiency of Si solar cells. Laser action in Ce^{3+} and Pr^{3+} ions doped δ-Al_2O_3 nanophosphors under cathode rays is likely to open new vistas of applications. Electroluminescent (EL) displays based on nanophosphors have shown higher resolution, lower power requirement and low voltage operation (~10 V). Nanophosphors can be used in generation of white light employing blue/UV emitting LEDs. Nanophosphors of ZnO and TiO_2 in cosmetics do have increased absorption of ultraviolet rays from sun but also add special tinge due to dopants. Bacteria-mediated delivery of nanophosphors and cargo into cells of live animals has been reported [3]. The sensitized emission of the acceptor is measured free of autofluorescence and scattered light in up conversion nanophosphors. The interferences of matrix absorption are almost completely eliminated as the donor is excited at near-infrared and the sensitized emission is measured at red or at far-red above the major absorption of both the oxy- and the deoxyhemoglobin as well as most of the other compounds present in any biological samples. No temporal resolution in detection is required, because the autofluorescence is completely absent and neither the acceptor generates any direct emission under near-infrared excitation [4].

1.4 Core Shell Nanoparticles

Colloidal core/shell nanostructure contains at least two semiconductor materials in an onion like structure. The basic optical properties of the core nanoparticles, for example, their

fluorescence wavelength, quantum yield, and lifetime, can be tuned by growing an epitaxial-type shell of another semiconductor. In such core/shell nanostructures, the shell provides a physical barrier between the optically active core and the surrounding medium, thus making them less sensitive to environmental changes, surface chemistry, and photo-oxidation. The shell further provides an efficient passivation of the surface trap states, giving rise to a strongly enhanced fluorescence quantum yield. This effect is a fundamental prerequisite for the use of nanocrystals in applications such as biological labelling and light-emitting devices, which rely on their emission properties [5]. Depending upon the energy level alignment the core shell structures can be classified in three categories viz. Type I, Type II and reverse Type I as shown in figure (1.4).

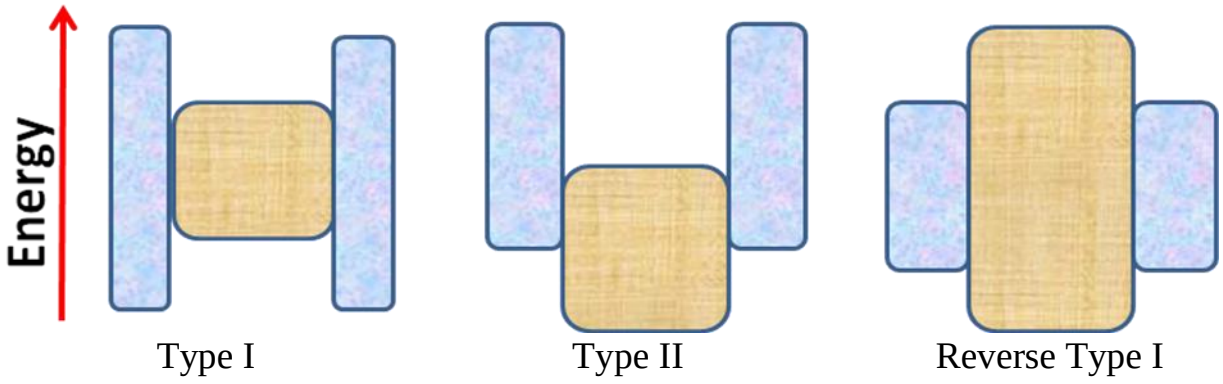

Figure 1.4 Schematic representation of the energy-level alignment in different core/shell systems. The upper and lower edges of the rectangles correspond to the positions of the conduction- and valence-band edge of the core (centre) and shell materials, respectively

In the former, the bandgap of the shell material is larger than that of the core and both electrons and holes are confined in the core. In the second, the bandgap of the shell material is smaller than that of the core and, depending of the thickness of the shell, the holes and electrons are partially or completely confined in the shell. In the latter, either the valence-band edge or the conduction band edge of the shell material is located in the bandgap of the core. Upon excitation of the nanocrystal, the resulting staggered band alignment leads to a spatial separation of the hole and the electron in different regions of the Core Shell structure. In type-I Core Shell structure, the shell is used to passivate the surface of the core with the goal to improve its optical properties. The shell of the structure physically separates the surface of the optically active core from its surrounding medium.

1.4.1 Type I core shell structure

Type I core/shell quantum dots have been shown to improve the stability and conversion efficiency of Quantum Dot-sensitized solar cells compared to core only Quantum Dots presence of oxygen or water molecules, is reduced. With respect to core nanocrystals, Core Shell systems exhibit generally enhanced stability against photodegradation. At the same time, shell growth reduces the number of surface dangling bonds, which can act as trap states for charge carriers and thereby reduce the fluorescence Quantum Efficiency. The first published prototype system was CdSe/ZnS. The ZnS shell significantly improves the fluorescence Quantum Efficiency and stability against photobleaching. Shell growth is accompanied by a small red shift (5–10 nm) of the excitonic peak in the UV/Vis absorption spectrum and the photoluminescence (PL) wavelength. This observation is attributed to a partial leakage of the exciton into the shell material.

1.4.2 Type II core shell structure

In type-II systems, shell growth aims at a significant redshift of the emission wavelength of the nanocrystals. The staggered band alignment leads to a smaller effective bandgap than each one of the constituting core and shell materials. The interest of these systems is the possibility to manipulate the shell thickness and thereby tune the emission colour towards spectral ranges, which are difficult to attain with other materials. Type- II nanocrystals have been developed in particular for near-infrared emission, using for example CdTe/CdSe or CdSe/ZnTe. In contrast to type-I systems, the PL decay times are longer in type-II NCs due to the lower overlap of the electron and hole wavefunctions. As one of the charge carriers (electron or hole) is located in the shell, an overgrowth of type- II Core Shell nanocrystals with an outer shell of an appropriate material can be used in the same way as in type-I systems to improve the fluorescence Quantum efficiency and photostability systems[5-7].

These core/shell nanocrystals are made of two semiconductor materials with a particular alignment of conduction and valence band edges at the interface, which Creates a step-like radial potential favouring the localization of one of the carriers in the core of a Quantum Dot and the other one in the shell. The resulting charge separation leads to a strong dipole moment, indirect band gap radiative emission, and a large offset between absorption and emission spectral profiles. It is thought that these fascinating properties would facilitate the use of Quantum Dots in several technological applications including photovoltaics, where spatial charge separation can increase the light conversion efficiency, biomedical labelling where the low overlap between emission and absorption energies of the dye eliminates the crosstalk phenomena, and Quantum Dot-based lasers, where photoinduced electric dipole

across the type II structure Stark shifts the biexciton level, resulting in a desirable linear amplification regime.

1.4.3 Reverse Type I core shell structure

In reverse type-I systems, a material with narrower bandgap is overgrown onto the core with wider bandgap. Charge carriers are at least partially delocalized in the shell and the emission wavelength can be tuned by the shell's thickness. Generally, a significant red-shift of the bandgap with the shell thickness is observed. The most extensively analyzed systems of this type are CdS/CdSe[8] and ZnSe/CdSe[9]. The resistance against photobleaching and the fluorescence Quantum Efficiency of these systems can be improved by the growth of a second shell of a larger-bandgap semiconductor on the core/shell nanocrystals [10].

1.4.4 Applications of Core shell nanophosphor

Core shell nanophosphors have varied applications in diverse fields viz. LED, Solar cell, Biomedicine etc. shell has an important effect, even when it is thin and takes a small portion of the total volume. For lossy dielectrics, the core-shell structure demonstrated frequency dependent behaviour and a window to tune the preferential orientation [11]. Nano-biological probes based on fluorescent core-shell NPs can be directed into single living cell to monitor the interested objects with high sensitivity and high selectivity. Primary or secondary antibodies or other special bimoleculars were covalently immobilized onto NPs' surface to recognize SmIgG+B lymphocyte for the immune-diagnosis of Systematical
Erythema Lupus[9], HepG liver cancer cells[12], ECV 304 cells and pacilitaxel induced early-stage apoptotic breast cancer cells[13]Targeted Drug Delivery is another area of application for core shell nanostructures. The particles have the ability to be conjugated to molecules without affecting the core and also can be used to encapsulate drugs. The material of choice decides the multifunctional nature of the particles .They can be structured so that they can be used for imaging and for drug delivery. the possibility of providing drug to the specific area has opened new vistas for the medical sciences however there are some phosphors which can readily be used for the cause but have toxic issues associated with them. By capping these phosphors with biocompatible materials makes them fit for human consumption and hence solve the problem of rejection by the human body. The separation of biological cells and life active species is a basic technique in biomedicine, such as the separation of foetal cells, separation of disease cells and classification of cells and so on.

Nanoparticles also offer a novel tool and means for the separation of cells and biological species [14].

1.5 II-VI semiconductor nanoparticles

Wide-bandgap II–VI compounds have been applied to optoelectronic devices, especially light-emitting devices in the short-wavelength region of visible light, because of their direct gap and suitable bandgap energies. Many methods have been extensively applied to grow high-quality films and bulk single crystals from the vapour and liquid phase. Here our focus is on ZnS and ZnO semiconductor which are studied in the present study.

1.5.1 ZnS: Crystal Structure

ZnS is a white- to yellow-colored powder or crystal. ZnS occur in both Zinc Blend and Wurtzite crystal structure. In the zinc blend (ZnS) structure, the space lattice is face centred cubic (FCC). There are two such FCC lattices which are separated by one quarter of the body diagonal of the unit cube. One lattice is occupied by Zn atoms, the other by S atoms as shown in fig 1.5 where yellow coloured spheres represent Zn atoms and purple represent sulphur atoms. Each atom has 4 nearest neighbours of the opposite kind and is bound to these 4 atoms which are arranged at the corners of the surrounding tetrahedron. The bonding is typically covalent.

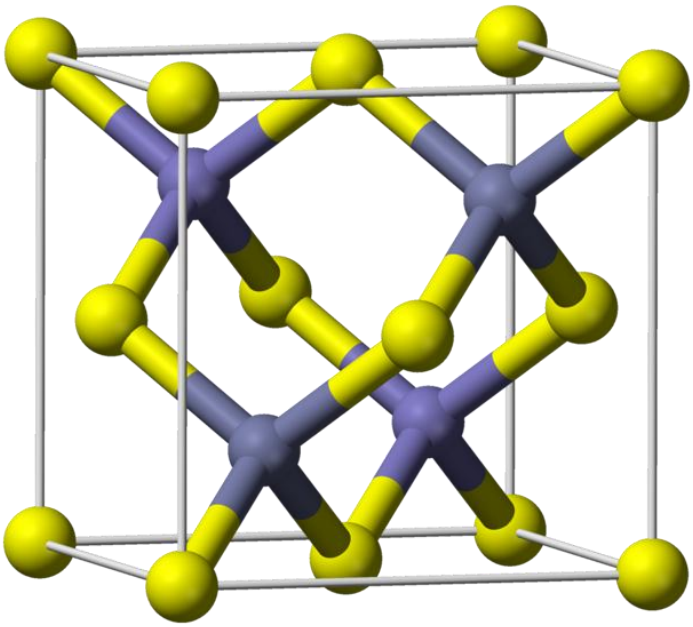

Figure 1.5 ZnS cubic Crystal Structure

1.5.2 ZnO: Crystal Structure

ZnO has a hexagonal wurtzite crystal structure, with lattice parameters a=3.25A° and c= 5.12A°. The Zn atoms are tetrahedrally coordinated with four O atoms, where the Zn d-electrons hybridize with the O-p electrons. The bonding between the Zn atoms and O atom are highly ionic, due to the large difference in their

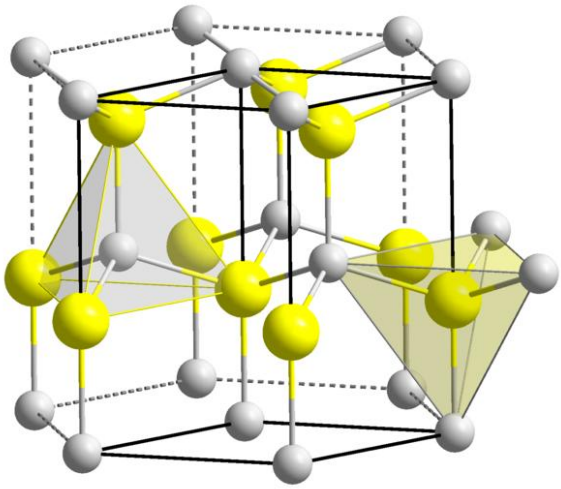

Figure 1.6 ZnO wurtzite crystal structure

electronegativity values(1.65 for Zn and 3.44 for O). Alternating Zn and O layers form the crystal structure as shown in fig 1.6 where yellow spheres represent O atoms and grey represents Zinc atoms. ZnO is a direct band gap semiconductor material with bandgap energy 3.37 eV, which makes it transparent in visible light and absorbing in the UV wavelength regions. Its exciton binding energy at room temperature is approx. 60 mev which is very high and hence enhances the luminescence efficiency of UV light emission. The room temperature electron hall mobility in single crystal ZnO is approx. 200 cm^2 V^{-1}. Nanostructures of ZnO such as nanowires and nanorods have been reported. Recent work of ZnO has shown ferromagnetism by doping with transition metal e.g., Mn with Curie temperature suitable for spintronic applications.

A Comparative study of properties of Zns and ZnO are given in table 1.

Table 1

	ZnS	ZnO
Melting point (K)	2038	2248
Energy gap E_g at 300K(eV)(ZB/WZ)	3.68/3.911	3.4
Structure	ZB/WZ	WZ
Bond length (A)	2.342 (WZ)	1.977 (WZ)
Lattice constant (ZB) a_0 at 300K (nm)	0.541	–
Density at 300K (g/cm^3)	ZB- 4.11 WZ-3.98	WZ-5.606
Lattice constant (WZ)at 300K (nm) $a0 = b0$ $c0$ $c0/a0$	 0.3811 0.6234 1.636	 0.32495 0.52069 1.602
Dielectric constant $\varepsilon_0/\varepsilon_\infty$	8.6/5.2	8.65/4.0
Electron effective mass ($m*/m0$)	–0.40	–0.27
Exciton binding energy(meV)	36	60

1.5.3 Applications of ZnS and ZnO

ZnS is a phosphor material used widely in displays, sensors, solar cells, lasers and electroluminescence. In optoelectronics, it finds use as light emitting diode, reflector, dielectric filter and window material [15]. Semiconducting nanomaterials are ubiquitous in device electronics, as their charge distribution can be manipulated desirably by applying voltage to perform the logic operations. ZnS nanoparticles have been used as electrode for electrochemical capacitor (EC) [16].

Zinc oxide finds applications in varistors which are used to prevent voltage surges in devices like mobile phones. Pigments in paints. Chinese white is a special grade of white pigment based on zinc oxide. A flux in ceramic glazes, where it can also help prevent crazing. A filler for rubber products and coatings for paper. Sunscreens and sunblocks for the prevention of sunburn due to its ability to absorb ultraviolet light

Chapter 2 Experimental

2.1 Synthesis Techniques

There are various methods for synthesizing nanoparticles. Here is a brief description of the various methods involved in nanophosphor synthesis.

1. Wet chemical synthesis

It is the simplest synthesis technique. The molecular motions and hence the chemical reaction may proceed very swiftly in the liquid state. However, the solvent molecules may remain as contaminants and this can adversely affect the performance of the phosphor. Another straight forward method is melting the constituents together thus obtaining the reactants in liquid phase without using a solvent. Again, there can be several difficulties in following this procedure. The melting points of the constituents like oxide are usually very high. The problem of obtaining a container that will withstand such high temperature without reacting with the constituents can prove insurmountable. The constituents themselves may have vastly differing melting points so that one of the constituents may vaporize well before reaching the melting point of the other.

2. Solid State Diffusion

In this method, the constituents are made to react through diffusion process. The temperature is just enough to have adequate diffusion to complete the reaction in laboratory time without melting the constituents. Reaction time and the temperature bear a sort of reciprocal reaction. It may not always be possible to lower the latter sufficiently .e.g. several aluminates cannot be formed even by the solid state diffusion at the temperatures below 1400 ºC.

3. Solvothermal method

To prepare some materials and its precursors, solvothermal method presents some advantages for several reasons. Solvothermal processes can be defined as chemical reactions or transformations in a solvent under supercritical conditions or near such a pressure-temperature domain. The specific physico-chemical properties of solvents in these conditions can, in particular, markedly improve the diffusion of chemical species. It is similar to

hydrothermal method but the pressures and temperatures involved are much lower. There is no need to use diamond anvil cell but the reactions can be performed in an autoclave. The solvents, the pressure-temperature criteria for the desired reactions are not known 'a priori' and starting from an `intelligent guess' the conditions are to be optimised.

4. Sol–gel method

It allows inorganic oxides and/or their immediate precursors to be produced from simple alkoxides or chelates via low temperature hydrolysis and condensation reactions. In sol-gel synthesis the reactants are obtained in very fine form so that the reaction time is greatly reduced, and one may obtained the products in reasonable time at lower reaction temperatures. The starting material, for example a metal salt, is converted in a chemical process to a dispersible oxide, which forms a colloidal dispersion (sol) on addition to dilute acid or H_2O. Removal of H_2O and/or anions from the sol produces a stiff gel in the form of spheres, fibres, fragments or coatings and this transition is usually reversible. Calcination of the gel in air yields an oxide product after decomposition of the salts.

2.2 Characterization techniques

There are various ways to study the behaviour of particles depending upon the type and nature of study. Here our main emphasis is on the structural, morphological, optical and magnetic properties of the material thus synthesized.

Here is a brief introduction of the instruments and the fundamental principle behind the technique involved

2.2.1 X-Ray Diffractometer

X-Ray Diffractometer is mainly used for the structural analysis of the samples prepared. In X-Ray Diffraction (XRD), a collimated beam of X rays, with wavelength λ~ 0.5-2A°, is incident on a specimen and is diffracted by the crystalline phases in the specimen [17].
Interaction of X-rays with sample creates secondary "diffracted" beams (actually generated in the form of cones) of X-rays related to interplanar spacings in the crystalline powder according to a mathematical relation called "Bragg's Law":

$$\mathbf{n\lambda = 2d \sin\theta}$$

where *n* is an integer

λ is the wavelength of the X-rays
d is the interplanar spacing generating the diffraction and
θ is the diffraction angle
λ and *d* are measured in the same units, usually angstroms

The intensity of the diffracted X-rays is measured as a function of the diffraction angle 2θ and the specimen's orientation. This diffraction pattern is used to identify the specimen's crystalline phases by matching it with standard data that is JCPDS card and to measure its structural properties, including strain (which is measured with great accuracy), epitaxy**,** and the size and orientation of crystallites (small crystalline regions). XRD can also determine concentration profiles, film thicknesses, and atomic arrangements in amorphous materials and multilayers. It also can characterize defects [18].

The X-Ray diffractometer consists of an X-Ray source, slits to adjust the shape of the beam, a sample, a detector and a goniometer for fine adjustment of the sample and the detector positions. X-rays are generated in a cathode ray tube by heating a filament to produce electrons, accelerating the electrons toward a target by applying a voltage, and bombarding the target material with electrons. When electrons have sufficient energy to dislodge inner shell electrons of the target material, characteristic X-ray spectra are produced. These spectra consist of several components, the most common being K_α and K_β. K_α consists, in part, of $K_{\alpha 1}$ and $K_{\alpha 2}$. $K_{\alpha 1}$ has a slightly shorter wavelength and twice the intensity as $K_{\alpha 2}$. The specific wavelengths are characteristic of the target material (Cu, Fe, Mo, and Cr). Filtering, by foils or crystal monochromators, is required to produce monochromatic X-rays needed for diffraction. $K_{\alpha 1}$ and $K_{\alpha 2}$ is sufficiently close in wavelength such that a weighted average of the two is used. Copper is the most common target material for single-crystal diffraction, with CuK_α radiation = 1.5418Å

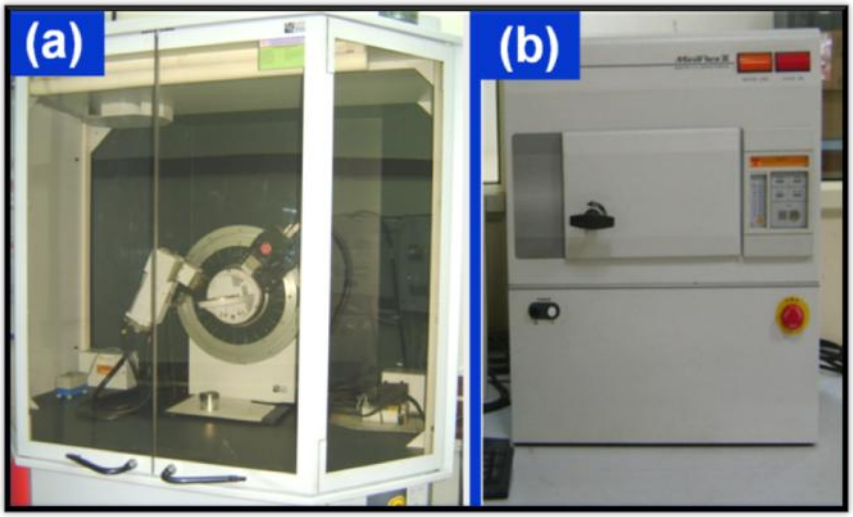

Figure 2.1 Picture of X-Ray Diffractometer

These X-rays are collimated and directed onto the sample. As the sample and detector are rotated, the intensity of the reflected X-rays is recorded. When the geometry of the incident X-rays impinging the sample satisfies the Bragg Equation, constructive interference occurs and a peak in intensity occurs. A detector records and processes this X-ray signal and converts the signal to a count rate which is then output to a device such as a printer or computer monitor. The geometry of an X-ray diffractometer is such that the sample rotates in the path of the collimated X-ray beam at an angle θ while the X-ray detector is mounted on an arm to collect the diffracted X-rays and rotates at an angle of 2θ.

2.2.2 Scanning Electron microscope

The SEM is a microscope that uses electrons instead of light to form an image. Since their development in the early 1950's, scanning electron microscopes have developed new areas of study in the medical and physical science communities. The SEM has allowed researchers to examine a much bigger variety of specimens. It produces a largely magnified image by using electrons instead of light to form an image. A beam of electrons is produced at the top of the microscope by an electron gun. The electron beam follows a vertical path through the microscope, which is held within a vacuum. The beam travels through electromagnetic fields and lenses, which focus the beam down toward the sample. Once the beam hits the sample, electrons and X-rays are ejected from the sample.

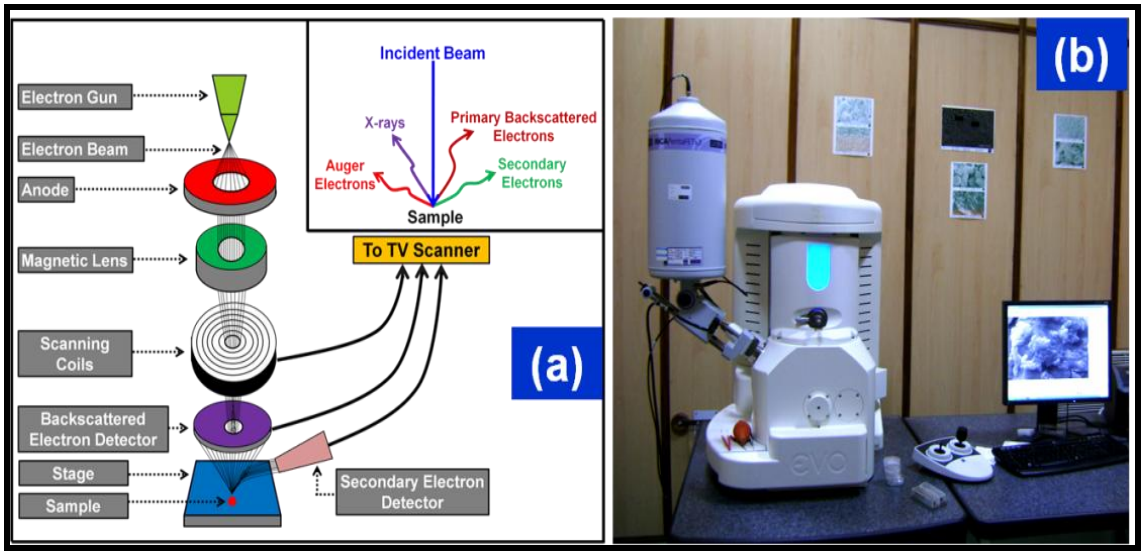

Figure 2.2(a) Schematic description of working of SEM (b) picture of SEM

Detectors collect these X-rays, backscattered electrons, and secondary electrons and convert them into a signal that is sent to a screen similar to a television screen. This produces the final image [19].

The scanning electron microscope has many advantages over traditional microscopes. The SEM has a large depth of field, which allows more of a specimen to be in focus at one time. The SEM also has much higher resolution, so closely spaced specimens can be magnified at much higher levels. Because the SEM uses electromagnets rather than lenses, the researcher has much more control in the degree of magnification. All of these advantages, as well as the actual strikingly clear images, make the scanning electron microscope one of the most useful instruments in research today

2.2.3 Transmission Electron Microscope

TEM works the same way as the light microscope except that it shines a beam of energetic electrons (like the light) through the specimen (like the slide). The use of electron instead of lights removes the resolution limitation due to the wavelength of light in case of a light microscope as the de Broglie wavelength of electron is much less than the light which makes it possible to get a thousand times better resolution.

Transmission electron microscope consists of

(1) Two or three condenser lenses to focus the electron beam on the sample

(2) An objective lens to form the diffraction in the back focal plane and the image of the sample in the image plane

(3) Some intermediate lenses to magnify the image or the diffraction pattern on the screen.

A "light source" at the top of the microscope emits the electrons that travel through vacuum in the column of the microscope. The condenser lens focuses the electrons into a very thin beam. The electron beam then travels through the specimen we want to study. Depending on the density of the material present, some of the electrons are scattered and disappear from the beam. At the bottom of the microscope the unscattered electrons hit a fluorescent screen, which gives rise to a "shadow image" of the specimen with its different parts displayed in varied darkness according to their density. The image can be studied directly by the operator or photographed with a camera.

Figure 2.3 Picture of TEM instrument

Diffracted electrons are observed in the form of a diffraction pattern beneath the specimen. This information is used to determine the atomic structure of the material in the sample. Transmitted electrons form images from small regions of sample that contain contrast, due to several scattering mechanisms associated with interactions between electrons and the atomic constituents of the sample. Analysis of transmitted electron images yields information both about atomic structure and about defects present in the material [20].

2.2.4 Photoluminescence

Photoluminescence spectroscopy is a contact-less, versatile, non-destructive method of probing the electronic structure of a material. A Laser beam impinges on a sample, where it is absorbed. The excess energy brought to the material can be dissipated through the emission of light, or luminescence. Photoluminescence (PL) is thus the spontaneous emission of light from a material under optical excitation. This light can be collected and analyzed spectrally, spatially and also temporally. In fact, PL spectroscopy gives information only on the low-lying energy levels of the investigated system. In semiconductor systems, the most common radiative transition is between states in the conduction and valence bands, with the energy difference being known as the bandgap. During a PL spectroscopy experiment, excitation is provided by laser/Xe light with an energy much larger than the optical bandgap. The photo-excited carriers consist of electrons and holes, which relax toward their respective band edges and recombine by emitting light at the energy of the bandgap. But, radiative transitions in semiconductors may also involve localized defects or impurity levels. In that case, the analysis of the PL spectrum leads to the identification of specific defects or impurities, and the magnitude of the PL signal allows determining their concentration. Finally, higher-energy optical transitions can be studied by means of photoluminescence excitation spectroscopy (PLE). In this latter configuration the detection is fixed on the emission line of the semiconductor system while the excitation light energy is varied. When it matches the energy of an optical transition in the absorption spectrum of the semiconductor, the PL signal increases. PLE is thus analogous to absorption spectroscopy and identical to it in the specific case where nonradiative relaxation processes are negligible. The recombination of the photo-excited carriers can involve both radiative and nonradiative processes. The respective rates of radiative and nonradiative recombination can be estimated from a careful analysis of the temperature variation of the PL intensity and PL decay time [21]. In semiconductor systems like quantum wells or quantum dots, the photoluminescence quantum yield is approximately constant up to temperatures of about 50-70K. At higher temperatures nonradiative recombination channels are activated and the PL intensity decreases exponentially. Apart the advantageous simplification of the underlying physics, low temperatures appear unavoidable for the optical study of semiconductor-based nanostructures [22].

In the present study following instruments were used for the optical characterization of the samples LS-55 luminescence spectrometer & Edinburgh Instruments combined steady state and time resolved luminescence Spectrometer.

Figure 2.4 Perkin Elmer LS 55 Luminescence Spectrometer

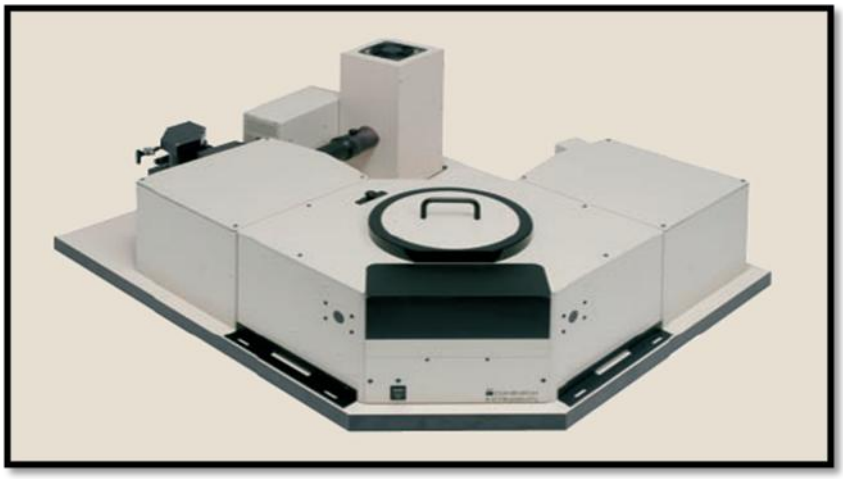

Figure 2.5 Edinburg spectrometer

The simple ray diagram of functioning of instrument is given in the Figure 6 . First of all excitation source, xenon flash lamp, is switched on. Energy from the source is focused by the spherical mirror onto the excitation monochromator. The majority of excitation beam is transmitted to the phosphor sample. The sample gets excited and energy emitted from it is once again focused by spherical mirror onto the emission monochromator. The angles of the gratings used in the excitation and emission monochromators are controlled by stepper motors. The emitted light is detected by a sensitive Photomultiplier tube (PMT) with high signal to noise ratio. The operation is software controlled. The excitation and emission wavelength (or range of excitation wavelengths in case of PL Excitation spectra or emission

wavelength in case of PL emission spectra), the excitation and emission slit width and wavelength scan speed can all be controlled through software. The resultant PL spectra are shown in a computer screen which can be saved and printed.

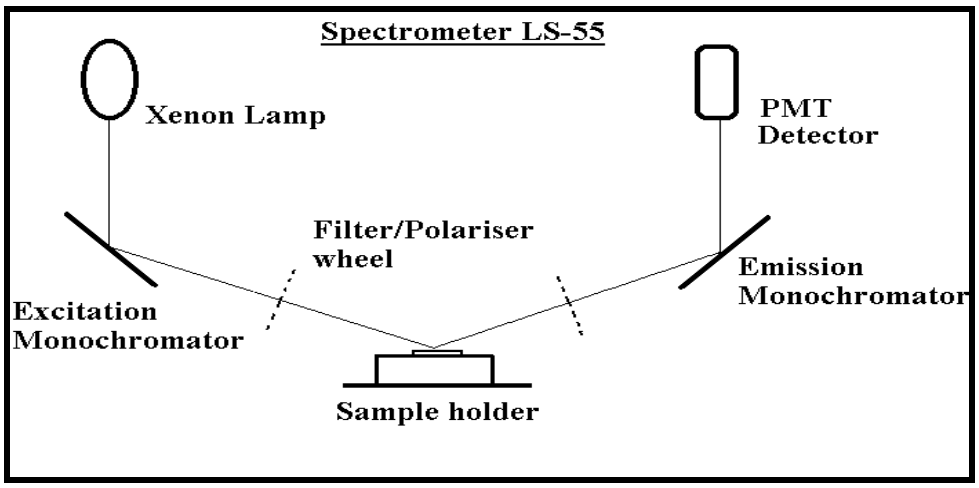

Figure 2.6 Functional Diagram of LS-55 Luminescence Spectrometer

The excitation and emission monochromators can be scanned over their ranges independently, synchronously or driven to selected points in their ranges. The spectral ranges of the monochromators are:

- Excitation monochromator 200 nm to 800 nm
- Emission monochromator 200 nm to 900 nm

2.2.5 Time Resolved decay study

Time resolved spectroscopy is an important tool for studying energy and charge transfer processes. The decay characteristics of phosphors could suggest the process of excitation and return to ground state and their time scale. It employs excitation by very short pulses of radiation like flash lamps, lasers etc, which can be spectrally tuned to the electronic transitions of the material to be studied [27]. The instrumentation for time-resolved spectroscopy is basically the same as for steady-state experiments. An excitation beam with a narrow wavelength range is directed at the sample, where it excites fluorescence. The fluorescence emission is collected at a 90º angle from the excitation to prevent light from the excitation source from interfering with the detection of the weaker fluorescence emission. The collected fluorescence emission enters the emission monochromator and the photon counts at particular emission wavelength are detected by the photomultiplier detector. The key differences for time-resolved spectroscopy are the replacement of the continuous light

source with a pulsed source. Time resolved studies were made using the Edinburg spectrophotometer which employs a time correlated single photon counting (TCSPC) technique.

2.2.6 UV-Visible Spectroscopy

Ultraviolet-visible (UV-Vis) spectroscopy is used to obtain the absorbance spectra of a sample in solution or as a solid. What is actually being observed spectroscopically is the absorbance of light energy or electromagnetic radiation, which excites electrons from the ground state to the first singlet excited state of the compound or material. The UV-Vis region of energy for the electromagnetic spectrum covers a wavelength range of 800 - 200 nm. The main Principle behind the absorbance spectroscopy is the Beer- Lambert Law [24].

$$A=\varepsilon bc$$

Where A is absorbance (unitless), ε is the molar absorptivity of the compound or molecule in solution ($M^{-1}cm^{-1}$), *b* is the path length of the cuvette or sample holder (usually 1 cm), and *c* is the concentration of the solution (M).Following instrument was used to measure the absorption and transmission spectra of the samples in the present study (Avantes Avaspec 3648)

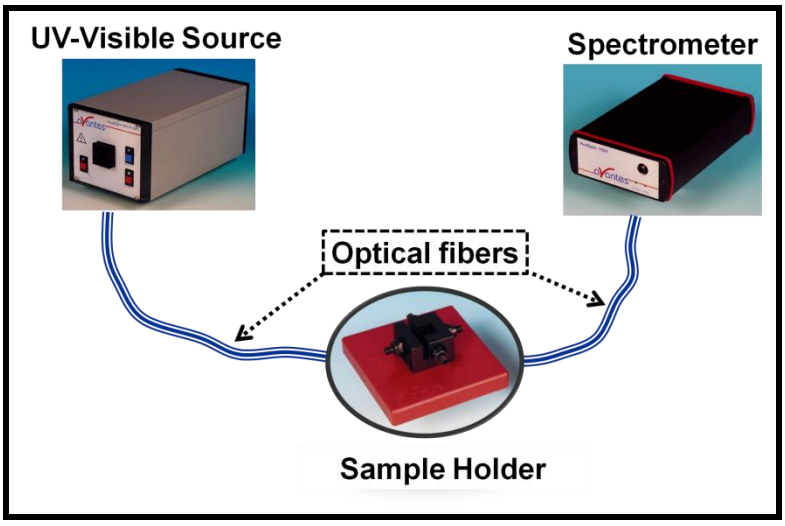

Figure 2.7 UV-VIS Spectrometer

The instrument has a light source, deuterium for ultra violet and tungsten for visible light, a sample holder and a Spectrometer.

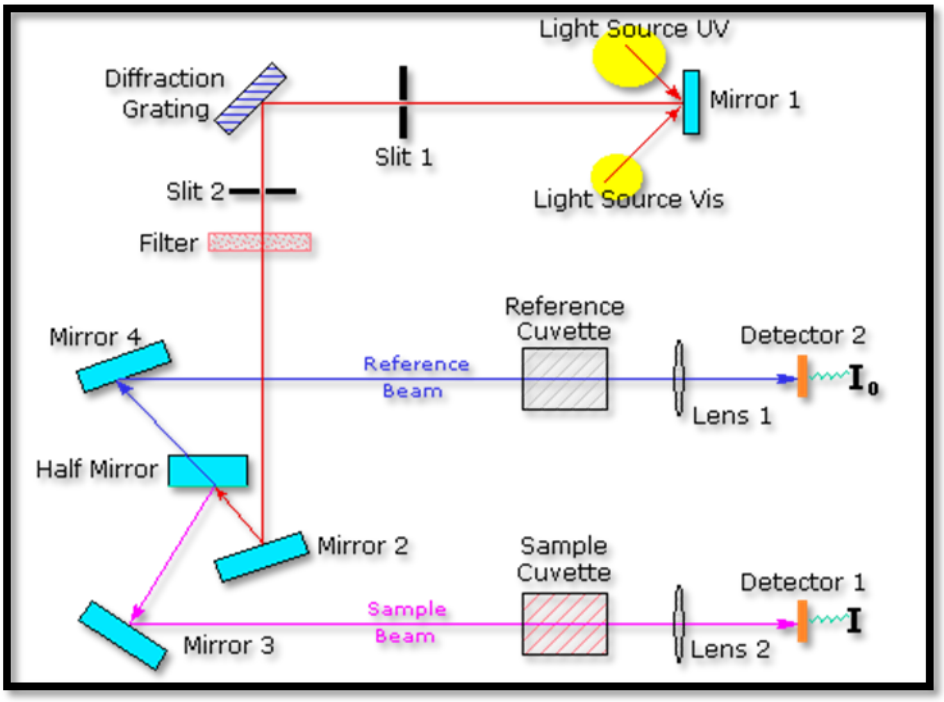

Figure 2.8 Optical Diagram of UV-Vis Spectrometer

A beam of light from a light source is separated into its component wavelengths by a prism or diffraction grating. Each monochromatic beam in turn is split into two equal intensity beams by a half-mirrored device. One beam, the sample beam (colored magenta), passes through a small transparent container (cuvette) containing a solution of the compound being studied in a transparent solvent. The other beam, the reference, passes through an identical cuvette containing only the solvent. The intensities of these light beams are then measured by electronic detectors and compared. The intensity of the reference beam, which should have suffered little or no light absorption, is defined as $\mathbf{I_0}$. The intensity of the sample beam is defined as **I**. Over a short period of time, the spectrometer automatically scans all the component wavelengths in the manner described. The ultraviolet (UV) region scanned is normally from 200 to 400 nm, and the visible portion is from 400 to 800 nm.

A Tauc plot is a convenient way of displaying the optical absorption spectrum of a material pioneered by J. Tauc, who proved that momentum is not conserved even in a direct optical transition. It is based on the relation between absorption coefficient(α) and the incident photon energy(hν) i.e.,

$$(\alpha h\nu) = A(h\nu - E_g)^n$$

Where A is a constant,Eg is the band gap of the material and the exponent n depends on the type of transition[26].

Typically, a Tauc plot shows the quantity hν (the energy of the light) on the abscissa and the quantity $(\alpha h\nu)^2$ on the ordinate, where α is the absorption coefficient of the material. The extrapolation of the linear portion of the curve to the X axis gives the value of bandgap.

2.2.7 Vibrating Sample Magnetometer

A vibrating sample magnetometer (VSM) operates on Faraday's Law of Induction, which tells us that a changing magnetic field will produce an electric field. This electric field can be measured and can tell us information about the changing magnetic field. A VSM is used to measure the magnetic behaviour of magnetic materials. Vibrating sample magnetometers (VSM) are used to characterize the DC magnetic properties of materials as a function of magnetic field, temperature, and time. The basic instrument includes the electromechanical system and the electronic system (including a personal computer[25]. The picture of VSM set up is shown in fig 2.9.

Figure2.9(a) Picture of VSM setup

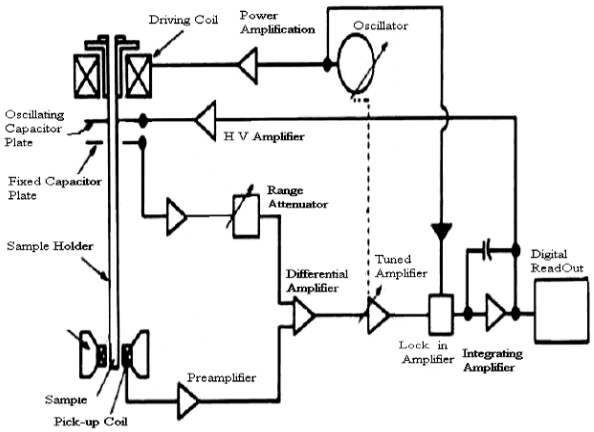

Figure 2.9(b) Block Diagram of a VSM

Working Principle

If a sample of any material is placed in a uniform magnetic field, created between the poles of a electromagnet, a dipole moment will be induced. If the sample vibrates with sinusoidal motion a sinusoidal electrical signal can be induced in suitable placed pick-up coils. The signal has the same frequency of vibration and its amplitude will be proportional to the magnetic moment, amplitude, and relative position with respect to the pick-up coils system.

The sample is fixed to a small sample holder located at the end of a sample rod mounted in a electromechanical transducer. The transducer is driven by a power amplifier which itself is driven by an oscillator at a frequency of 90 Hz. So, the sample vibrates along the Z axis perpendicular to the magnetizing field. The latter induced a signal in the pick-up coil system that is fed to a differential amplifier. The output of the differential amplifier is subsequently fed into a tuned amplifier and an internal lock-in amplifier that receives a reference signal supplied by the oscillator. The output of this lock-in amplifier, or the output of the magnetometer itself, is a DC signal proportional to the magnetic moment of the sample being studied.

Chapter 3 ZnS Quantum Dots

Quantum Dots exhibit broad excitation, narrow emission and high photostability. There has been a considerable emphasis on synthesis of Quantum Dot containing heavy metals, including CdSe and CdS etc, which usually show high fluorescent efficiency. However there is a toxicological issue associated with them. The methods used for synthesizing Quantum Dots are also very complex, here we have synthesized ZnS Quantum Dots where Zn has no such toxicological issue associated with it by a simple wet chemical method.

3.1 Synthesis

3.1.1 Undoped ZnS Quantum Dots

Precursors Used:

Following Precursors were used for the synthesis of ZnS quantum Dot

Sodium Sulphide	**Zinc Chloride**
Molecular Formula- Na_2S	Molecular Formula- $ZnCl_2$
Molecular Weight- 136.28g	Molecular Weight-78.04g
Physical state- crystal form	Physical State- Solid Flakes
Colour-White	Colour-Yellow
Company- Loba Chemie	Company- Loba Chemie
Solvent	
Isopropanol	

Synthesis Procedure

Step 1- 0.05 M Solution of Zinc Chloride was prepared in Isopropanol with continuous stirring at 40^0C for 40 min

Step2- 0.05M solution of Sodium Sulfide in Isopropanol was prepared with continuous stirring at 30^0C for 50 min

Step3- Both the solutions were mixed with continuous stirring for 30 min

Step4- White coloured precipitates thus formed were centrifuged and were further washed with ethanol many times

Step 5- Finally the precipitates were dried in an Oven at 90° for 1 hour.

3.1.2 ZnS doped with magnetic impurity (Cr)

ZnS Quantum dots were doped with different concentrations of Chromium.

Precursors used

Zinc Chloride	Sodium Sulphide
Molecular Formula-$ZnCl_2$	Molecular Formula-Na_2S
Molecular weight-136.28g	Molecular Weight-78.04g
Physical state- Crystalline Powder	Physical state- Solid Flakes
Colour- White	Colour-Yellow
Company-Loaba Chemicals	Company- Loaba Chemicals
Chromium Sulphate	**Solvents**
Molecular Weight-392.183g	Isopropanol
Physical state-Solid Powder	Deionized Water
Colour-Green	
Company-Fine Chemicals	

Synthesis Procedure

As the samples with different doping concentration of Chromium were to be synthesized stock solution was prepared beforehand. Method of Preparation of solution A, B and C is given below

Solution A- 0.05 M Solution of Zinc Chloride was prepared in Isopropanol with continuous stirring at 40^0C for 40 min

Solution B- 0.05M solution of Sodium Sulfide in Isopropanol was prepared with continuous stirring at 30^0C for 50 min

Solution C- 0.05 M solution of Chromium Sulphate was prepared in Deionized Water

The steps involved in the process are depicted in the Diagram below with the picture of samples with varied doping Concentrations

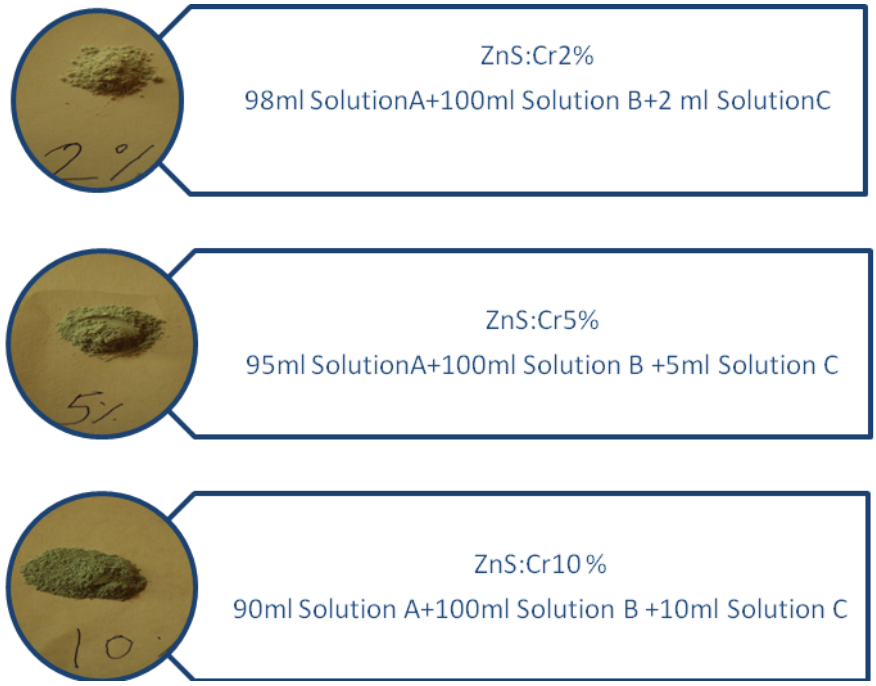

After mixing the desired amount of solution the resultant solution was centrifuged at 5000 rpm for 15 minutes. It was washed with ethanol to remove any undesired impurity and at last was kept in an oven for drying at 90° for 1 Hour. The body colour of the sample changed with the doping concentration as shown in the picture above.

3.2 Result and Discussion

3.2.1 Structural Analysis: XRD

The aim of the analysis is to identify the crystalline phase of the synthesized material by matching it with the standard data (JCPDS). Here the instrument used is a Rigaku Miniflex X-ray Diffractometer using the principle of Bragg Brantano Geometry, with Cu-Kα radiation(λ=1.54 A°). 2θ was scanned in the range 20° to 80°

3.2.1.1 Undoped ZnS

The XRD Pattern of undoped ZnS nanoparticles prepared by wet Chemical method is shown in Figure3.1. It shows formation of well crystalline perfect cubic phase of ZnS. The three major peaks at 28.7°, 47.6° and 56.4° corresponds to (111), (220) and (311) planes of cubic ZnS Zinc blend structure and is in well agreement with the standard data i.e., Joint Committee

on Powder Diffraction Standards (JCPDS card No. - (80-5520)). The purity of sample can be well determined by the XRD as there are no extra peaks other than diffraction peaks corresponding to ZnS. Washing the synthesized product with ethanol many times is important for the removal of any unwanted impurity.

The peak broadening indicates that the average particle size of the prepared sample is very small and is further established by the calculation of its particle size from the width of the XRD peak by using the Deby Scherrer Formula i.e.,

$$D = K\lambda/\beta\cos\theta$$

Where D is the mean grain size, K is a geometric factor, λ is the X-ray wavelength, β is the FWHM of diffraction peak and θ is the diffraction angle.

The particle size calculated from the XRD data is 2.5nm which is less than the Bohr radius of the ZnS hence stating that the ZnS particle thus formed is a Quantum Dot (QD). The Lattice constant determined using the values of (hkl) and d spacing recorded from the XRD is shown in Table at the end of the chapter which again matches with the standard results.

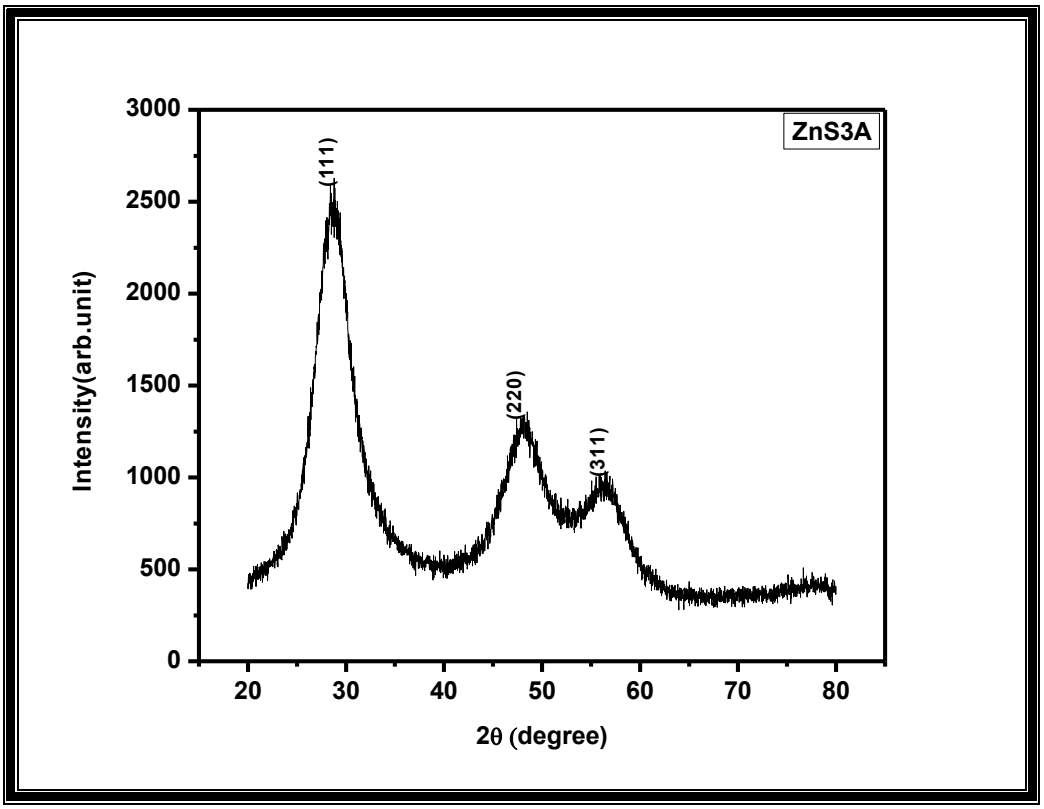

Figure 3.1 XRD Pattern of undoped ZnS Quantum Dots

The XRD spectra of ZnS QDs synthesized with slight variation in total reaction time is shown in Fig.2.

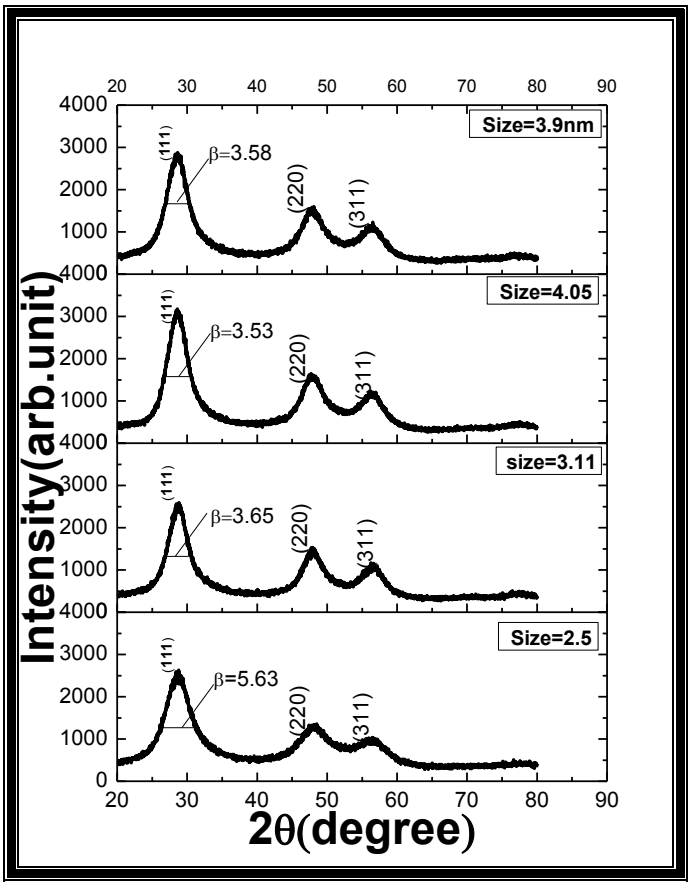

Figure 3.2 XRD pattern of ZnS with Different particle size

The decrease in peak broadening with the increase in particle size can be clearly seen from the Figure 3.2.The FWHM from the XRD Data of (a), (b),(c),(d) is 3.58,3.53,3.65,5.63 giving particle size 3.9,4.05,3.11 and 2.5 nm respectively. It can also be seen that peak height increases with increase in particle size.

The variation in particle size is a direct effect of change in reaction time and the ripening time of the sample. It has been observed that the increase in ripening time results in particles of larger size.

3.2.1.2 Cr doped ZnS

The ZnS QDs were doped with Chromium with different doping concentrations i.e. 1, 2, 5 and 10 %. The XRD pattern of ZnS doped with 2% and 5% doping concentration of Chromium is shown in Fig.3.3. The three major peaks of ZnS are very well formed as seen in

the XRD pattern although there is a slight change in the intensity of the peaks with the doping of the impurity indicating that increasing amount of Cr doping in ZnS QDs deteriorates the crystalline order.

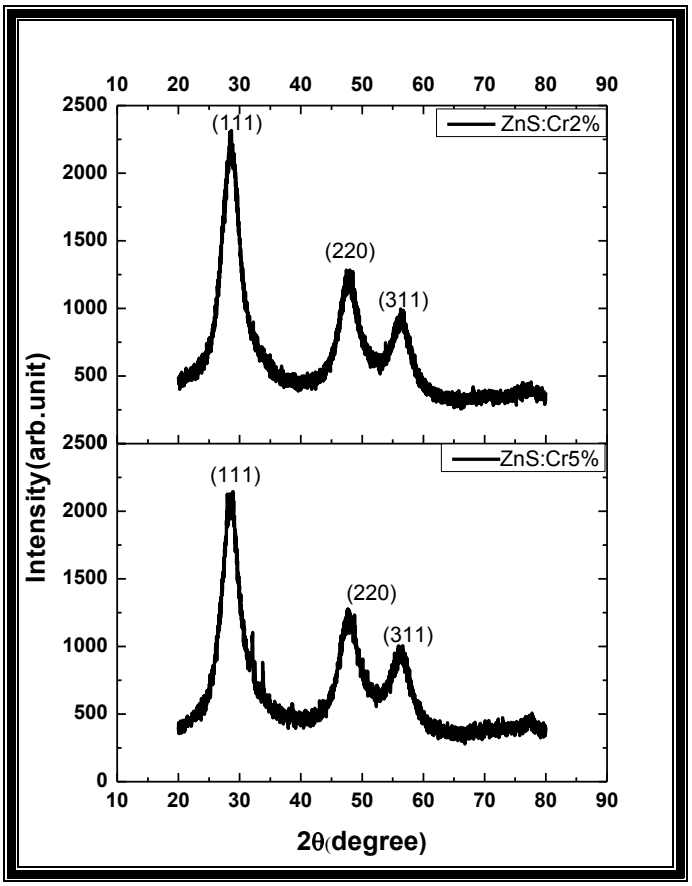

Figure 3.3 XRD Pattern of ZnS doped with Chromium Concentration 2% and 5%

3.2.2 Morphological Study:

It is very important to study the size and shape of the synthesized nanoparticles/ QDs. The morphological study of the doped and undoped ZnS quantum dots were done through Scanning Electron Microscope Images and Transmission Electron Microscope Images. SEM images were taken using a LEO 440 PC based digital scanning electron microscope.

(a) Scanning Electron Microscopy:

The SEM images of ZnS doped with 5% chromium are shown below with different magnifications viz. 5X, 10X, 20X, 50X.

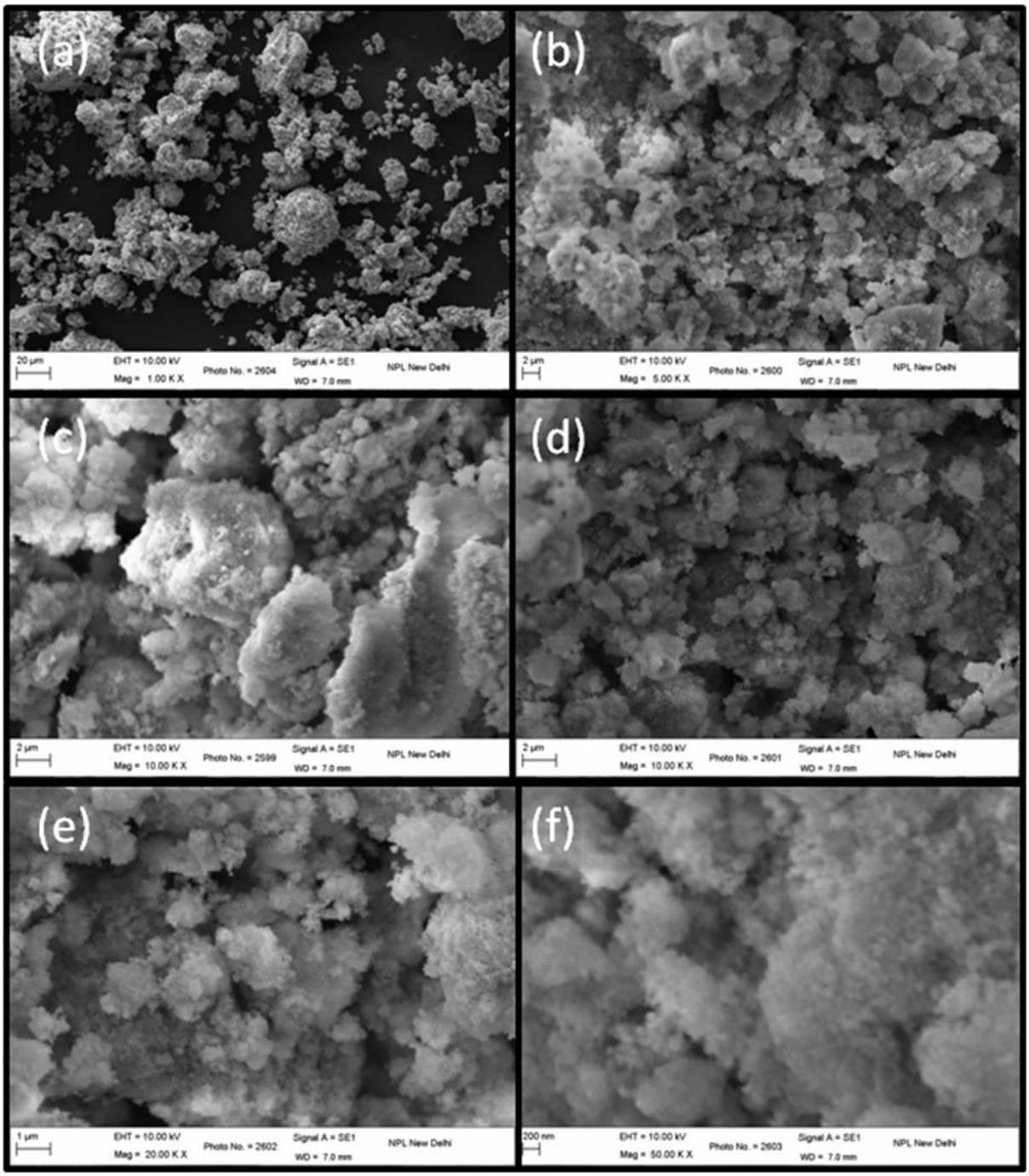

Figure 3.4 SEM images of ZnS doped with chromium

The SEM images show a picture of agglomerated particle. The particles are very small and hence are not comprehendible from the SEM images. Hence High Resolution Transmission Microscopy became essential.

(b) Transmission Electron Microscope

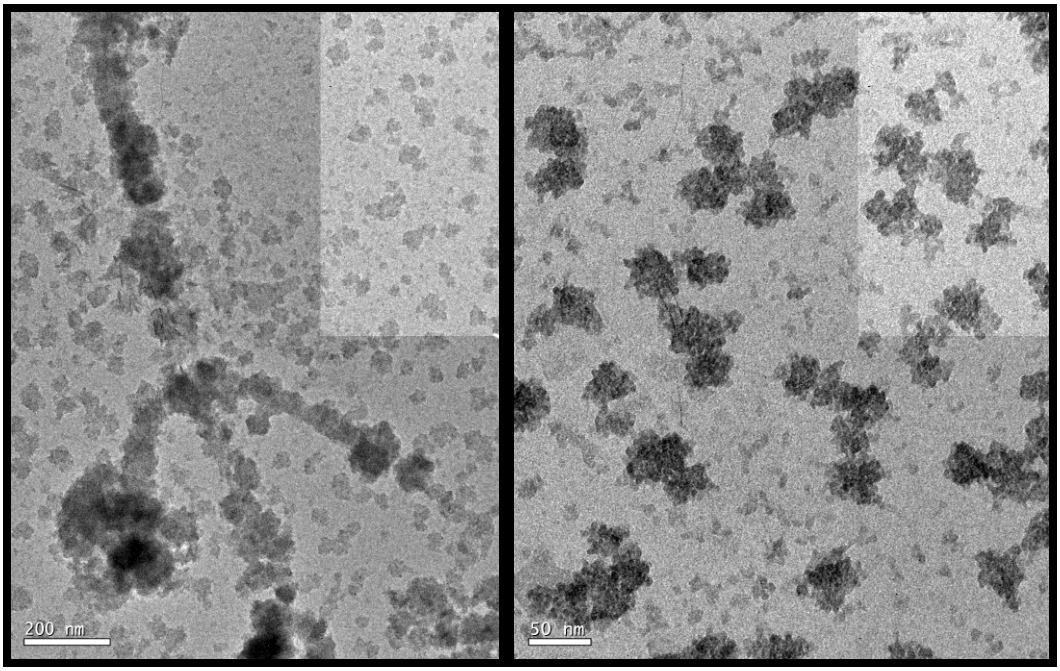

Figure 3.5 HRTEM images of ZnS Quantum Dots with scale bars(a)200nm (b) 50 nm

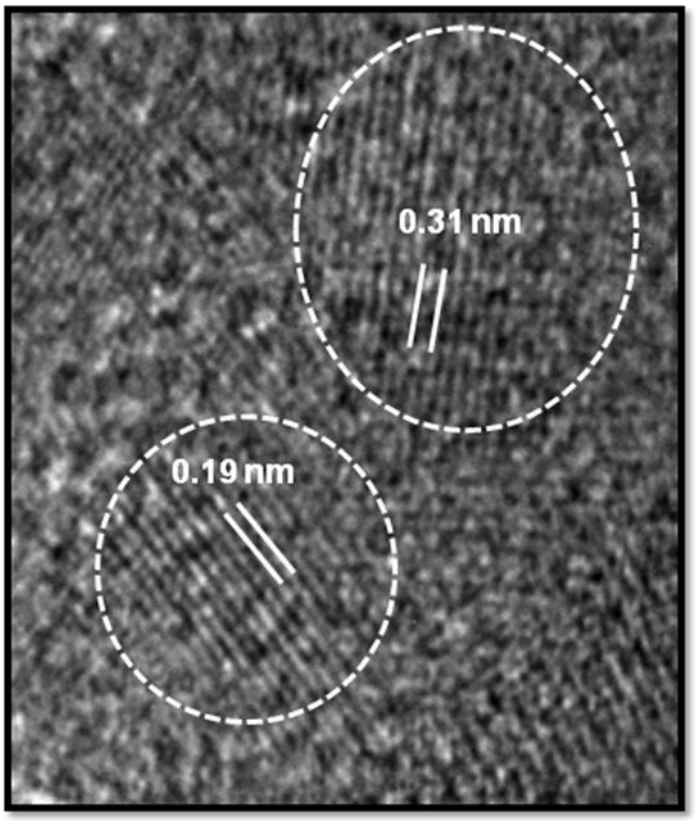

Figure 3.5(c) HRTEM images of ZnS quantum Dot

The TEM images of Figure 3.5(a) and (b) show a combination of agglomerated and isolated particles with denser part consisting of ZnS agglomerates and lighter shaded region because

of isolated particles. Agglomeration is caused as the reaction time was quite high paving way for Ostwald ripening also there is absence of any type of surfactant which could possibly avoid agglomeration. The high resolution TEM image (Fig.3.5c) clearly shows the individual particles (as shown by dotted area) and the lattice planes. The planar spacing obtained from TEM images is 0.31 nm and 0.19 nm as shown in figure 5c corresponding to the (111) and (220) planes respectively of ZnS cubic structure as reported in JCPDS (Card- 80-5520). Nearly Spherical shape was observed for the isolated particles with most of the particle growth in mainly (111) direction. The particle size, orientation of lattice planes and interplanar spacing obtained from HRTEM image all match perfectly well with obtained XRD data.

3.2.3 Optical Properties:

The optical properties of the quantum dots are studied through Photoluminescence spectra, Time Resolved Spectroscopy and UV-Visible spectroscopy.

(a) Photoluminescence (PL)

Photoluminescence excitation (PLE) as well as emission spectra was recorded for undoped and Cr doped ZnS QDs. PLE gives the photo absorption characteristics of the QD ensemble when the emission is recorded at a particular wavelength. Hence an indication of blue shift in PLE compared to bulk ZnS band gap gives an indication of a quantum confinement effect.

Undoped ZnS QD

PL excitation spectra of undoped ZnS QDs is shown in Fig. 3.6 (red curve). The excitation spectra peaks at 330 nm (3.76eV) which indicates a blue shift from the bulk ZnS fundamental absorption edge or the exciton position. ZnS quantum dot were excited by Xenon lamp at 330 nm and the PL emission spectra is shown in Fig.6 (black curve). The emission from undoped ZnS QDs are in blue (440 nm) and arises from intrinsic point defects.

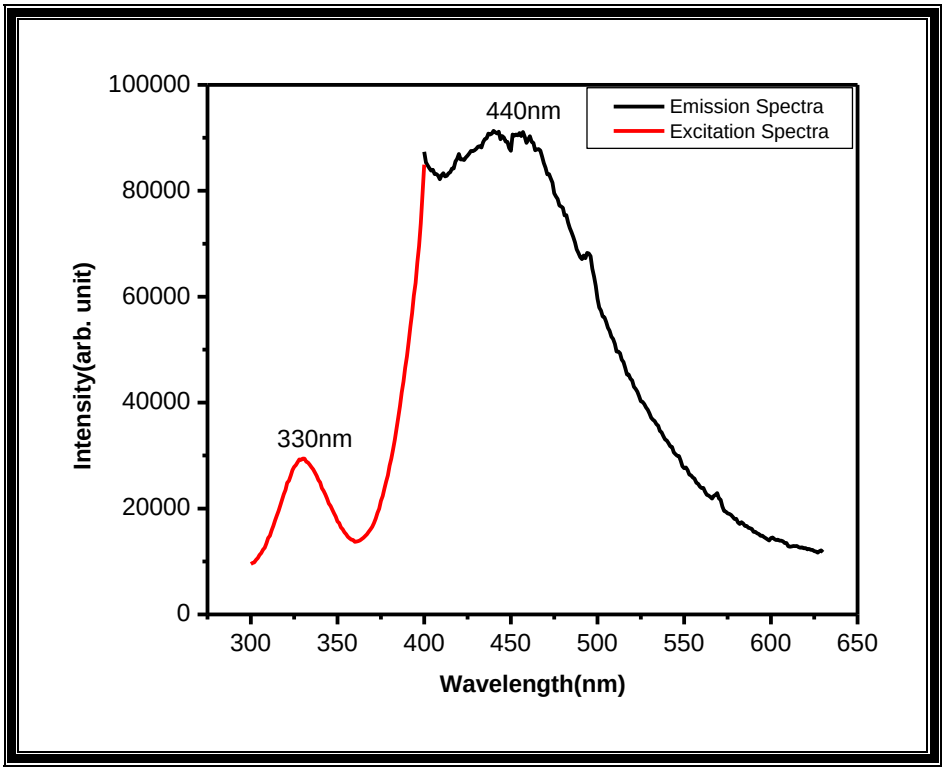

Figure 3.6 PL Emission and excitation Spectra of ZnS Quantum Dot

The energy level diagram showing two possible point defects namely sulphur vacancy (S^{2-}) and zinc vacancy (Zn^{2+}) as well as surface states due to dangling bonds and all possible recombination processes are shown in Fig.3.7.

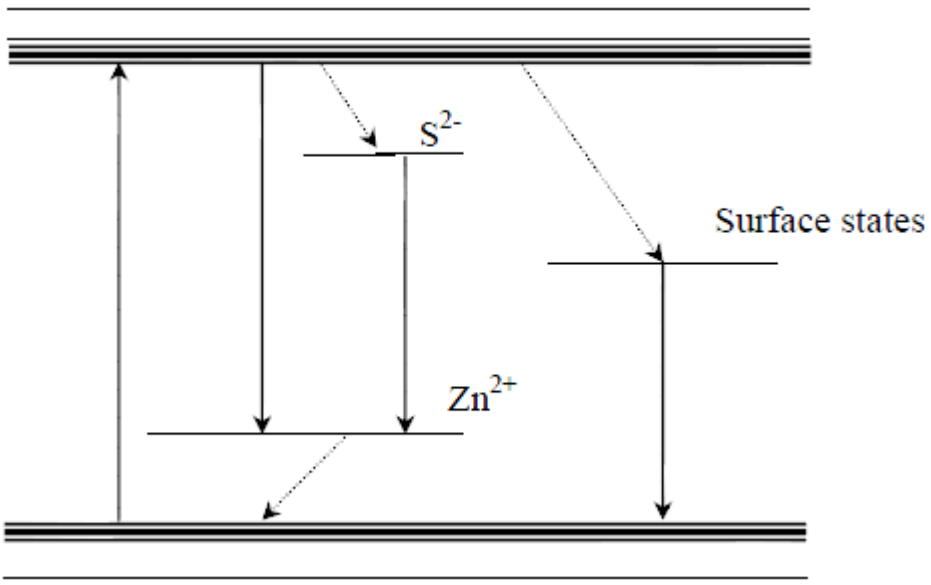

Figure 3.7 Energy level Diagram of ZnS nanoparticles

It can be understood from the energy level diagram shown in Figure 3.7 that the energy states within the band gap in the QDs are produced due to surface states due to dangling bonds or due to vacancies of sulphur or zinc atoms. The blue luminescence in ZnS has been conventionally attributed to a zinc vacancy centre charge compensated by either a monovalent anion (e.g.,Cl^-) or trivalent cation (e.g.,Al^{3+}). Photons of higher energy (3.75eV) excite the electrons from the valance band (VB) which reaches the conduction band (CB). The excited electrons decay non-radiatively to donor/surface-states and then decay radiatively to acceptor level/ valance band and emit a photon of lower energy (2.81eV). As the particle size is very less there is a further blue shift in the emission wavelength i.e. of shorter wavelength. From the PL emission peak the blue shift to 439 nm can be clearly seen as the bulk ZnS emit at 450nm this is because as the particle size decreases, the valance band edge shifts downwards. Therefore, the emitted photon has comparatively higher energy giving photoluminescence peak at shorter wavelength.

Cr doped ZnS QDs

The PL excitation spectra of ZnS doped with varying concentration of Cr is shown in Fig.3.8. The excitation spectra of undoped ZnS at the same emission wavelength (467 nm) is also included for comparison. It can be clearly seen that the band edge excitation peak at 330 nm gradually decreases with Cr doping in ZnS and only the excitation peak at 311 nm becomes prominent in Cr doped samples. The corresponding PL emission spectra is shown in Fig.3.9 at an excitation wavelength of 311nm. From the PL Emission spectra of ZnS doped with Cr of different concentration viz. 1,2,5 and10 %, it can be seen that the intensity of the broad blue emission from undoped ZnS peaking at 440 nm decreases continuously with Cr doping. Also the peak intensity at 467 nm decreases as the concentration of Chromium increases in ZnS lattice.

The PL measurements indicate that the characteristic peak due to Cr is not observed in the ZnS:Cr QDs. Instead, Cr doping decreases the PL intensity. XRD results also showed deterioration in crystallinity due to Cr doping. Such type of behaviour can arise when the PL originates due to intrinsic point defects/surface states and due to Cr doping, such defects decreases in number. Thus Cr affects the luminescence properties of ZnS indirectly.

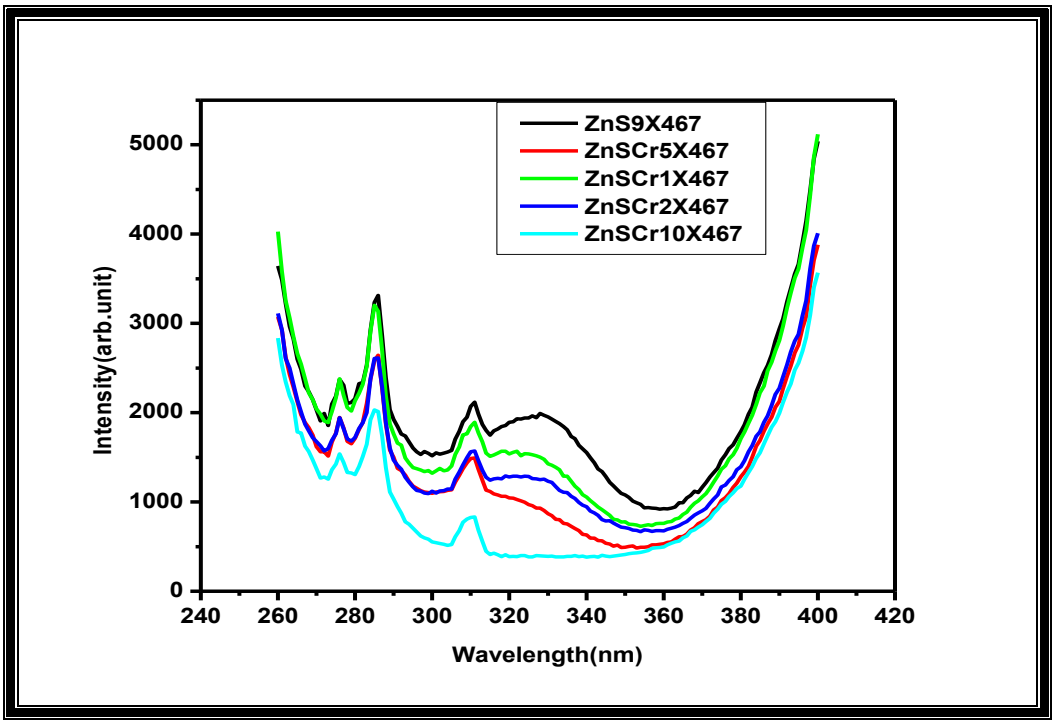

Figure 3.8 Pl Excitation spectra of ZnS doped with different Chromium Concentration

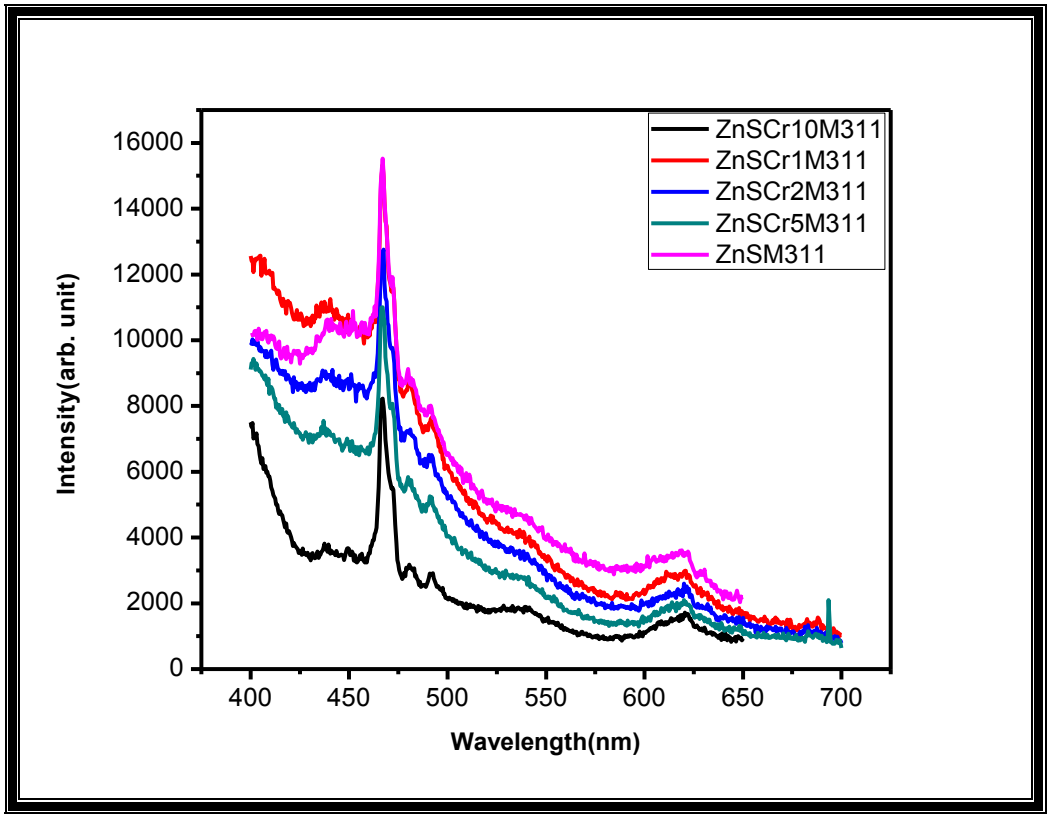

Figure 3.9 PL Emission spectra at Excitation of 311nm of ZnS doped with different concentration of Chromium

(b) Time Resolved Spectroscopy

Time resolved decay of luminescence provides the temporal scale in which the luminescence recombination process takes place within the material system.

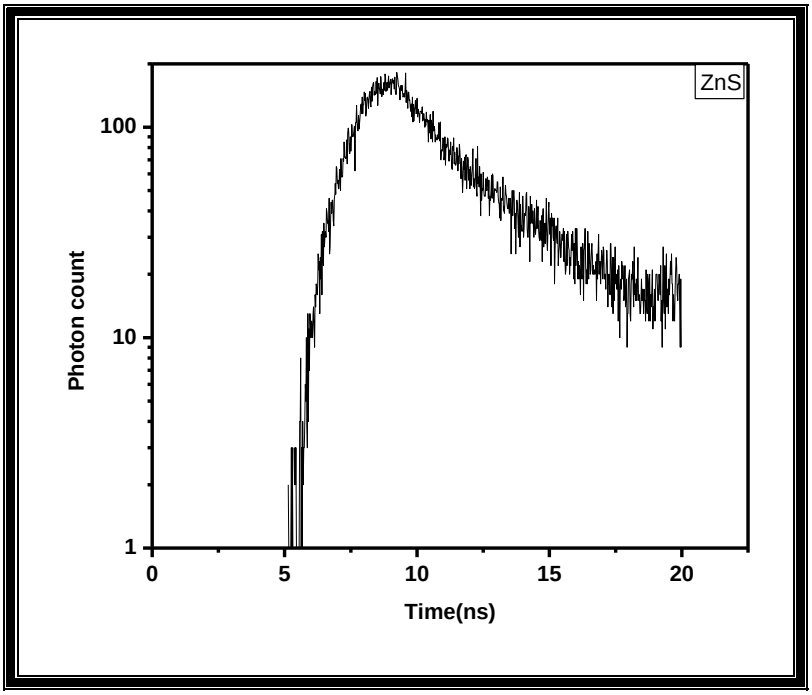

Figure 3.10Time resolved luminescence decay curve for ZnS Quantum Dot Excited at 330nm

The luminescence decay curve of undoped ZnS QDs is shown in Fig. 3.10. The decay curve for ZnS quantum Dot for excitation wavelength of 330 nm and emission at 440 nm could be fitted into a single exponential with a decay time (1/e) of 2.36 ns. The decay parameters are listed in table I. The goodness of fit is indicated by the value of χ^2 which should ideally be 1. Such short decay time indicates excitonic recombination.

Table I

Decay parameters

T	2.3686$\pm$ 0.092ns
Fit=A+$B_1e^{(-t/\tau_1)}$	
A	17.405
χ^2	1.026

Here τ i.e. characteristic lifetime denotes the time taken to decay from the beginning of the decay to 37% of the original value, B_i a pre exponential factor, which includes both

instrumental and sample parameters. In a multiexponential decay, concentration ratio of individual components can be inferred from values of B_i.

(c) UV-Visible Spectroscopy

UV-Visible absorption and transmission spectra of ZnS QDs suspended as colloid in glycerol medium has been recorded. The absorption spectra and transmission spectra are shown respectively in Fig.3.11 and 3.12.

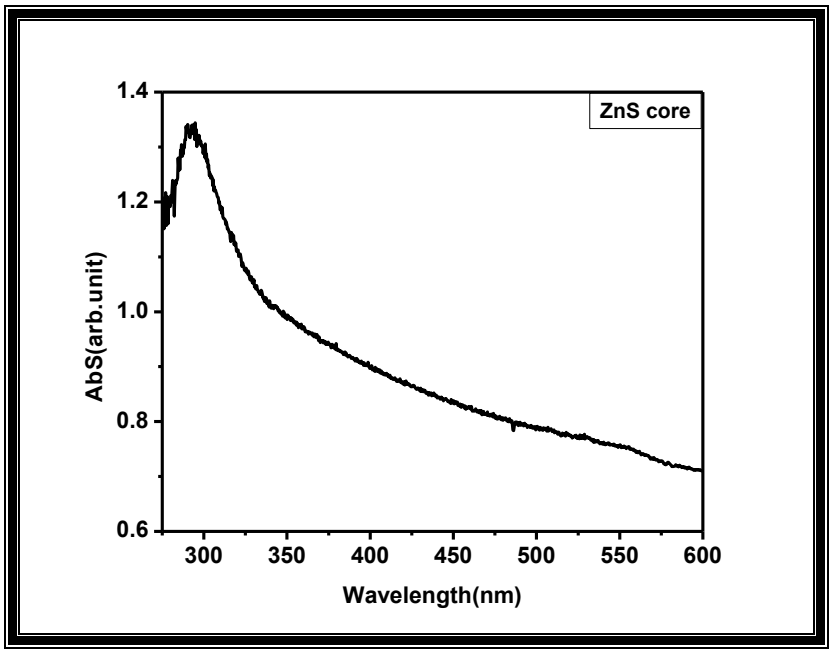

Figure 3.11 Absorption Spectra of ZnS

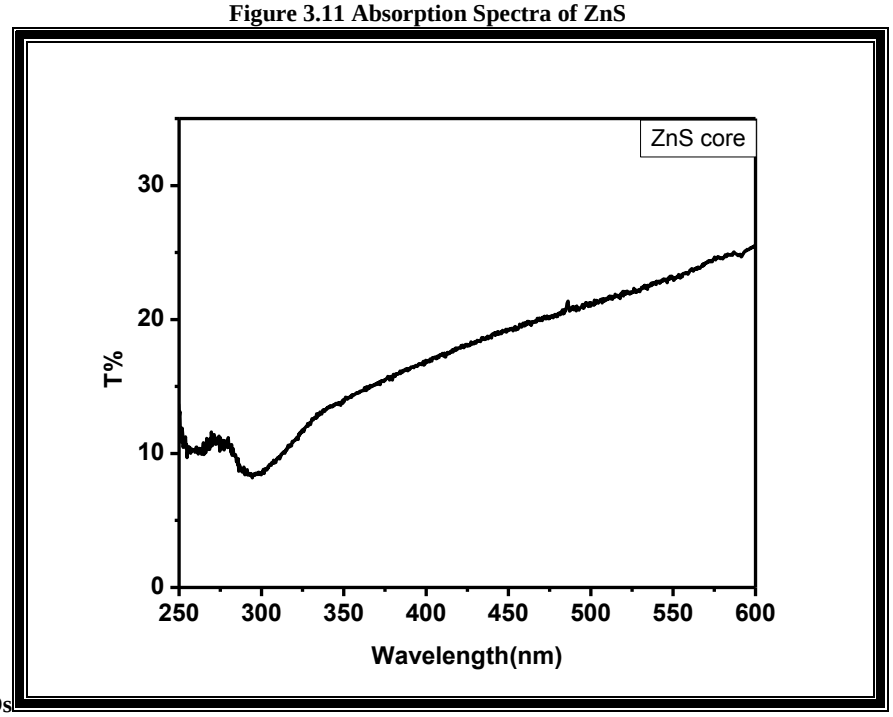

QDs

Figure 3.12 Transmission Spectra of ZnS QDs

Theoretical Band gap Calculation

Using the Brus equation for change in band gap energy with the change in particle size i.e. $E_g=E_{gbulk}+h_2/4r^2(1/m_e*)$ where E_{gbulk} for ZnS is 3.67eV.the size of the quantum Dots were estimated For the particle of size 2.5nm the band gap energy calculated is 4.024eV

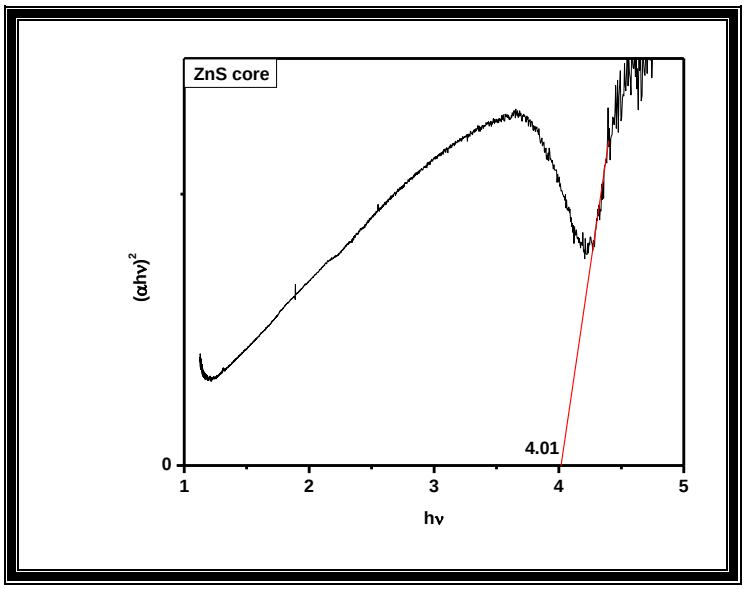

Figure 3.13 Tauc Plot of ZnS QDs. The band gap is estimated from the intercept in the energy axis.

The tauc plot of a direct band gap semiconductor ZnS is plotted from the measured absorption coefficient as shown in Fig.3.13. The band gap derived from extrapolating the linear portion of the tauc plot is 4.01 eV. The band gap of bulk ZnS is 3.67 eV but with the decrease in particle size it has increased to 4.01 eV which clearly shows the quantum confinement effect for the 2.5 nm ZnS QDs. As the exciton Bohr radius of ZnS is 5 nm, the observed quantum confinement effect for the 2.5 nm ZnS QDs is as per theoretical predictions.

3.2.4 Magnetic Properties

Magnetic properties of ZnS doped with magnetic impurity Cr was studied through magnetization curve measured with Vibrating Sample Magnetometer (VSM). Chromium is remarkable for its magnetic properties: it is the only elemental solid which shows antiferromagnetic ordering at room temperature (and below). Above 38 °C, it transforms into a paramagnetic state.

Magnetization curves of ZnS doped with different concentration of Chromium were studied and as can be seen from the graphs above with the increase in doping concentration from 1 % to 5% there is a shift from diamagnetic behaviour to paramagnetic one. Room temperature magnetization curves of ZnS:Cr are shown in Fig. 3.14 -3.16.

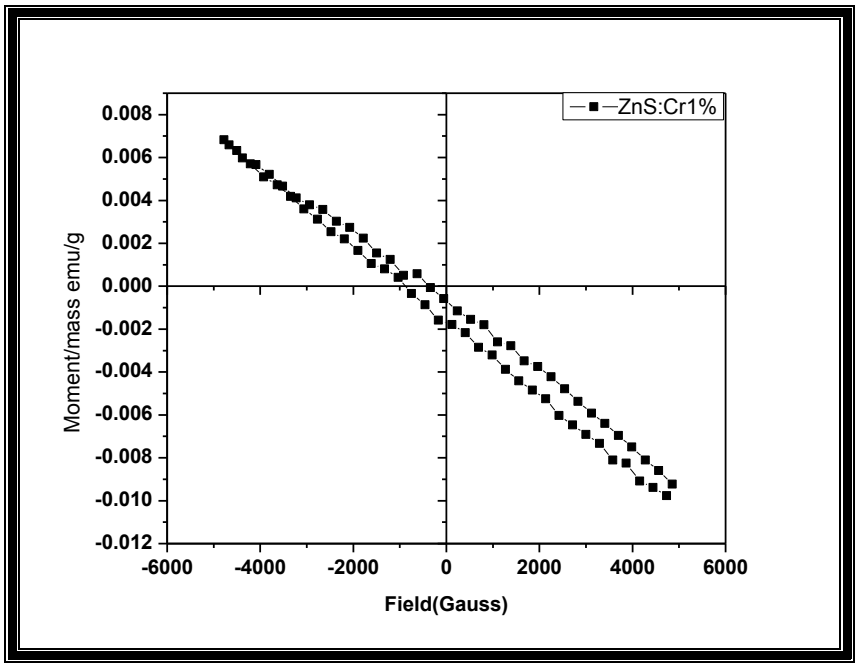

Figure 3.14 Magnetization curve for ZnS:Cr

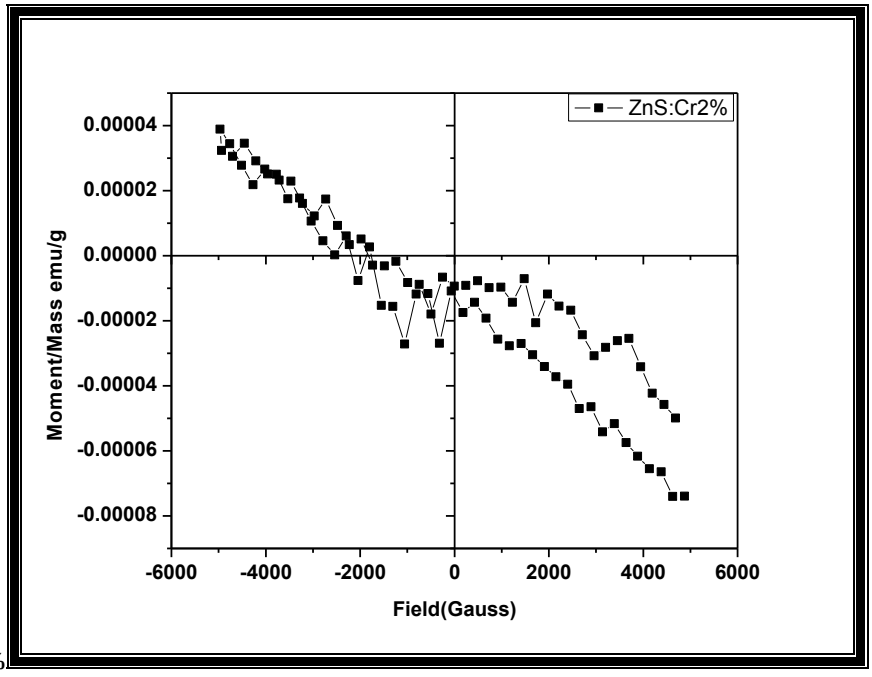

1%

Figure 3.15 Magnetization Curve for ZnS:Cr 2%

In order to see whether magnetic behaviour changes at low temperature, magnetization curve has been recorded at 80 K for ZnS:Cr (5%) QDs that exhibited paramagnetic behaviour at room temperature. The low temperature magnetization curve is shown in Fig. 3.16(b). It can be clearly seen that maximum magnetization at 80 K has increased to 90 memu/g compared to 2.5 memu/g at room temperature.

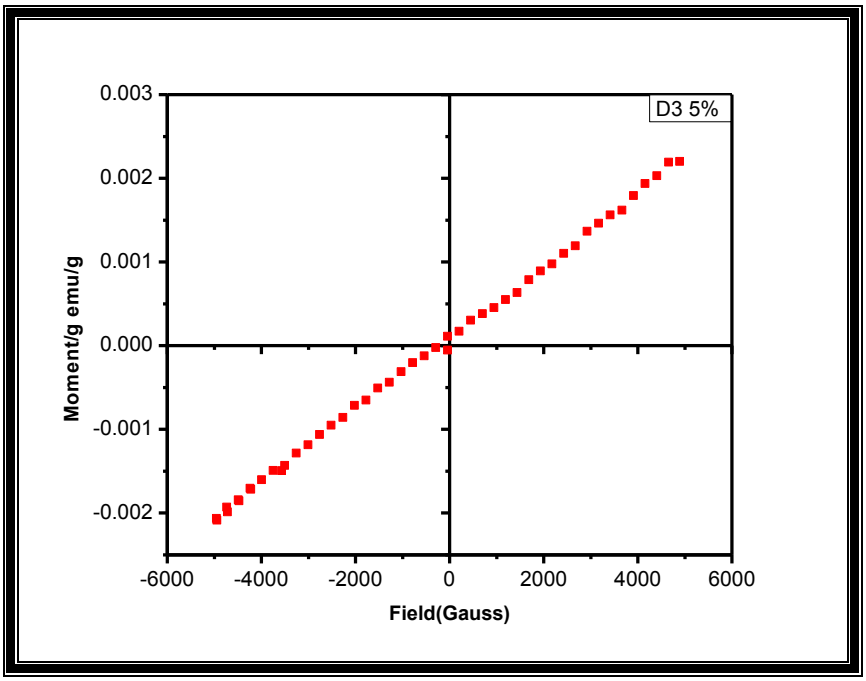

3.16(a)

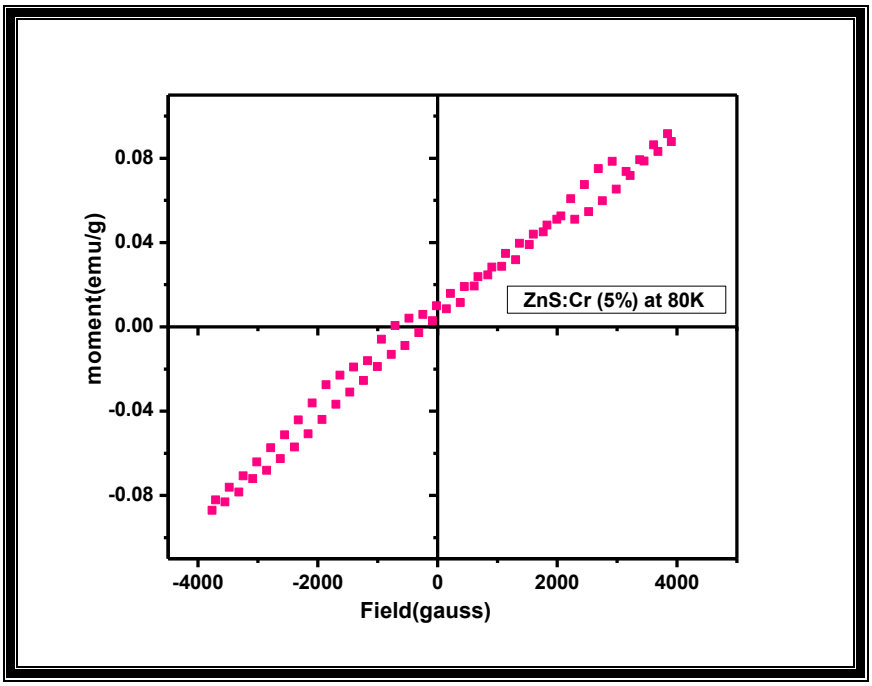

3.16(b)

Figure 3.16 Magnetization Curve for ZnS:Cr 5% at (a) room temperature and (b) 80 K

3.3 Conclusions:

ZnS Quantum Dots were successfully synthesized using the simple wet chemical method. The reaction time is a critical parameter in the synthesis process as it paves way for agglomeration as well as increase the size of the particle significantly. The size of the particle is below the exciton Bohr radius of ZnS as confirmed by both XRD and TEM. The optical characterization

revealed the nature of the luminescence property and effect of both particle size and doping concentration. A blue shift in PL indicated the decreased particle size effect Band Gap calculated with the help of UV-Vis spectroscopy in confirmation with the theoretical calculation using brus formula gives an idea how there is an increase in Band gap with the particle size and manifestation of quantum confinement effect in the synthesized ZnS QDs. Doping with magnetic impurity Cr introduces magnetic behaviour in diamagnetic ZnS and there is a shift from diamagnetic to paramagnetic behaviour of the particles with increase in Cr concentration. Further enhancement in magnetization has been observed at lower temperature.

Chapter 4 ZnS/ZnO Core Shell Quantum dot

The luminescence efficiency of ZnS nanoparticles may be lower due to the increased surface area and higher unsaturated dangling bond related nonradiative recombination sites or some other kinds of dead layers due to surface defects. Now in order to overcome this, an inorganic capping of ZnS is a possible solution. Here the synthesis of ZnS/ZnO core shell nanostructure via a simple wet chemical route is described.

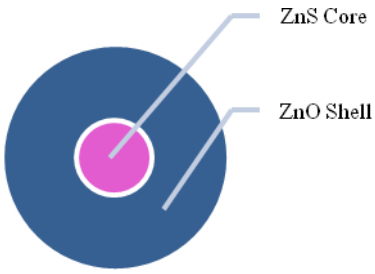

The inorganic capping saturates dangling bonds and substantially reduce nonradiative centres (dead layers). Moreover, they can also withstand high temperature treatments and electron bombardment without increasing the ZnS particle size or time dependent luminescence degradation (or aging effects).

4.1 Synthesis

4.1.1 Undoped Core with Undoped Shell

ZnS Quantum Dot	ZnO Shell
0.2g ZnS QDs (as synthesized)	Zinc Acetate (C_2H_5OOZn)
particle size- 2.5nm	Molecular Weight-219.49g
Colour- White	Physical State- White Powder
	Company-Loba Chemi
Solvent: Deionized water	

Double Diluted Ammonia

Synthesis Procedure

Step1 0.045M zinc acetate solution was prepared in D.I water

Step2 As prepared quantum dot were mixed in the solution of Step 1 on a magnetic stirrer

Step 3 Double Diluted Ammonia was added and pH 10 was maintained for shell growth

Step 4 The resulting Mixture was centrifuged and kept for drying in an oven at 90^0 for 24 Hours.

4.1.2 Undoped ZnS Core with Cr Doped Shell

Precursor used

Zinc Acetate	**Chromium Sulphate**
Molecular formula-C_2H_5COOZn	Molecular formula-Cr_2SO_4
Molecular weight-219.49g	Molecular Weight- 392.183g
Physical State- Crystalline Powder	Physical state- Powder
Colour- white	Colour-Green
Solvent	
Deionized Water	

Synthesis Procedure

Step1 0.045M zinc Acetate solution was prepared in water

Step2 As prepared ZnS quantum dot were added and stirred

Step3 Chromium Sulphate solution was added in the above solution

Step4 Double diluted ammonia was added till the pH 10 was obtained

Step5 The resulting mixture was centrifuged and dried at 90^0 for 24 hours.

4.1.3 Cr Doped ZnS Core with Cr Doped ZnO Shell

Same procedure was repeated with the difference that here ZnS doped with Cr was used.

4.2 Result and Discussion

4.2.1 Structural Analysis: XRD

4.2.1.1 Undoped ZnS Core/ undoped ZnO Shell

The XRD pattern of undoped ZnS Core with undoped ZnO shell is shown in Fig.4.1

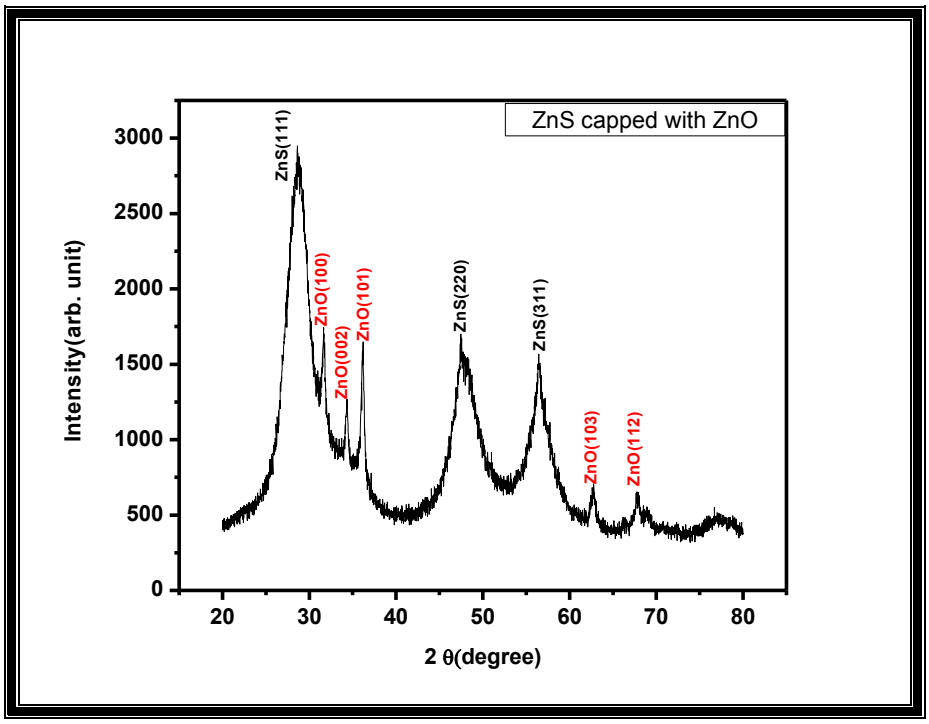

Figure 4.1 XRD pattern of Undoped ZnS Core with Undoped ZnO shell. The sharp peaks coming from ZnO shell is clearly discernible.

Along with the three major peaks at 28.7°, 47.6° and 56.4° corresponding to (111), (220), (311) Planes of Cubic ZnS Zinc blend structure there are five more peaks at 31.1°,34.3°,36.1°,62.7°,67.9° which corresponds to (100),(002),(101),(103) and (112) respectively of ZnO hexagonal structure in well agreement with the standard data i.e., Joint Committee on Powder Diffraction Standards (JCPDS card No. - (89-1397)).

The presence of Both ZnS and ZnO peaks in the XRD indicates the successful formation of hexagonal phase ZnO shell on ZnS cubic core.

4.2.1.2 Undoped ZnS Core/ Cr doped ZnO Shell

The XRD pattern of undoped ZnS Core with Cr doped ZnO shell is shown in figure 4.2

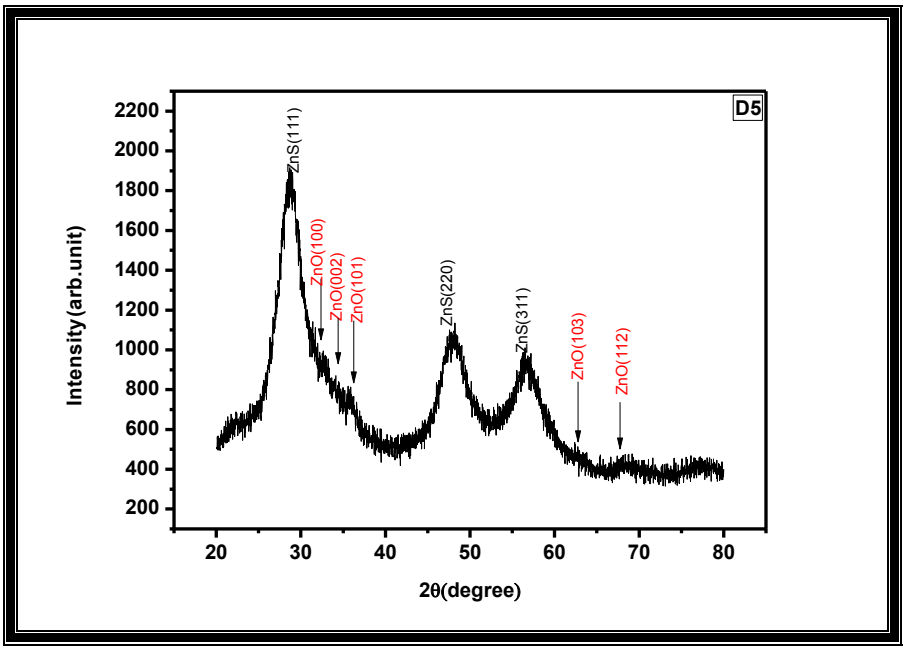

Figure 4.2 XRD pattern for undoped ZnS core with Doped ZnO shell

In addition to the ZnS core XRD peaks, indication of peaks due to ZnO: Cr shell is visible. The lower diffracted intensity of peaks from ZnO: Cr shell may be due to smaller shell thickness or poorer crystallinity due to Cr doping.

4.2.1.3 Cr doped ZnS Core/ Cr doped ZnO Shell

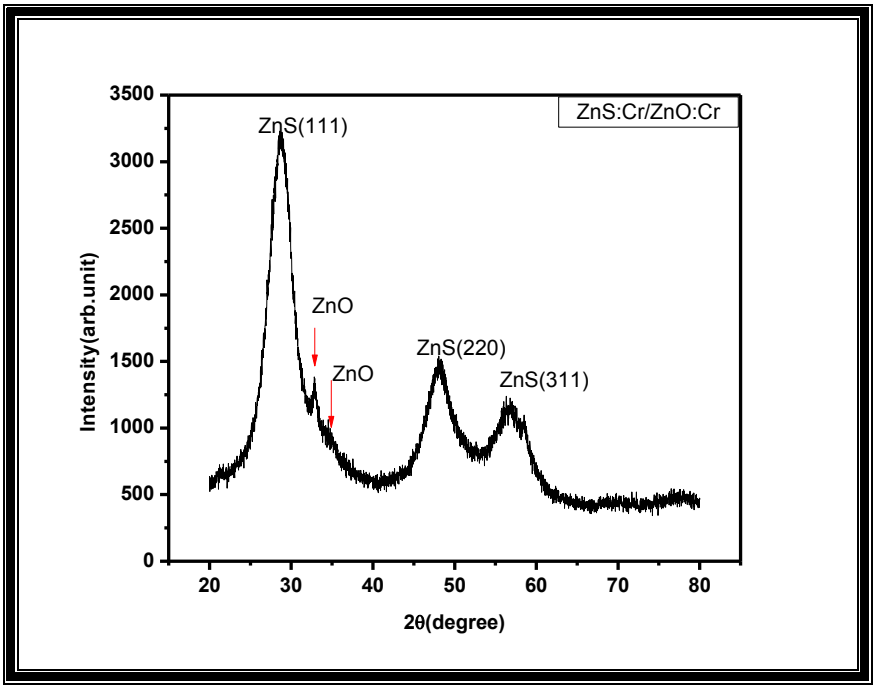

Figure 4.3 XRD pattern of Doped ZnS core and doped ZnO shell

Here, in addition to ZnS peaks some hints of ZnO peaks are also seen and hence indicate the presence of both ZnS and ZnO phase in the nanostructure.

4.2.2 Scanning Electron Microscope (SEM)

The SEM images of undoped ZnS Core with doped ZnO shell are shown in figure 4.4 (a-i) with different magnification. The individual particles are very small and are not discernible even with the highest magnification used in SEM. Agglomeration of very small particles can, however, be seen.

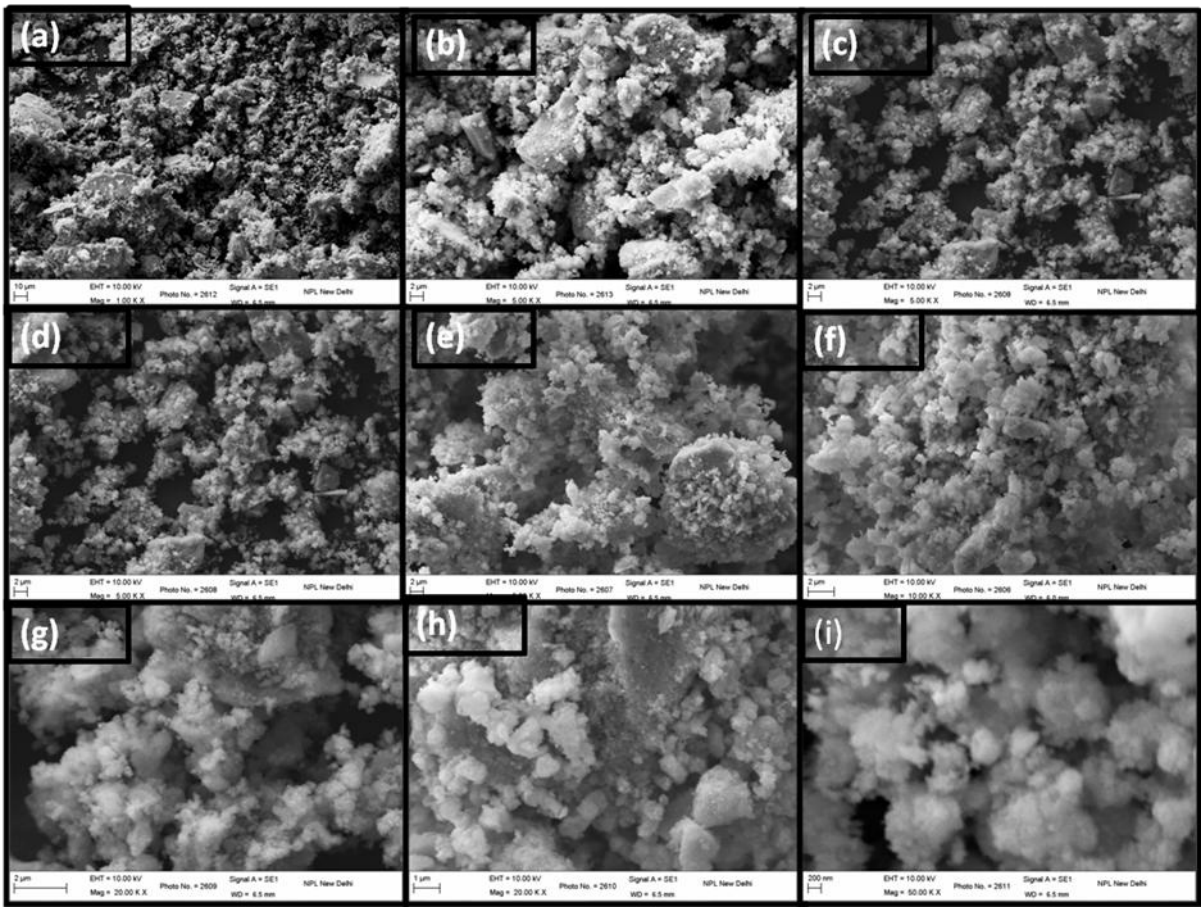

Figure 4.4 SEM image of undoped ZnS Core with doped ZnO shell taken at different magnifications

4.2.3 Transmission Electron Microscopy (TEM)

The particles are not discernible in the SEM images because of the size of the particles, TEM images however gives a clear picture of the smallest of particle at atomic scale. In order to study the Morphology of nanoparticles synthesized, Transmission electron Microscopy was employed. Here are the TEM images shown in figure4.5(a) and (b) taken at different resolution showing agglomerated particles The lattice fringes of both core and shell particles

when taken at higher resolution are shown in Fig.4.6(a)-(c) followed by interpretation of the same.

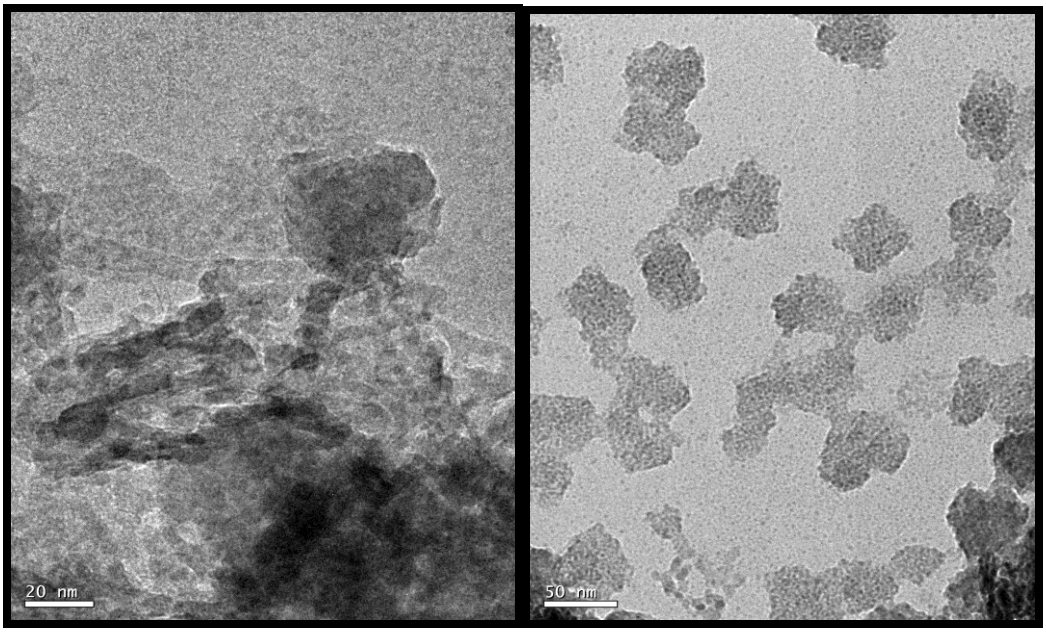

(a) **(b)**

Figure4.5 TEM image of ZnS/ZnO nanostructure with scale bars (a) 20nm and (b) 50nm

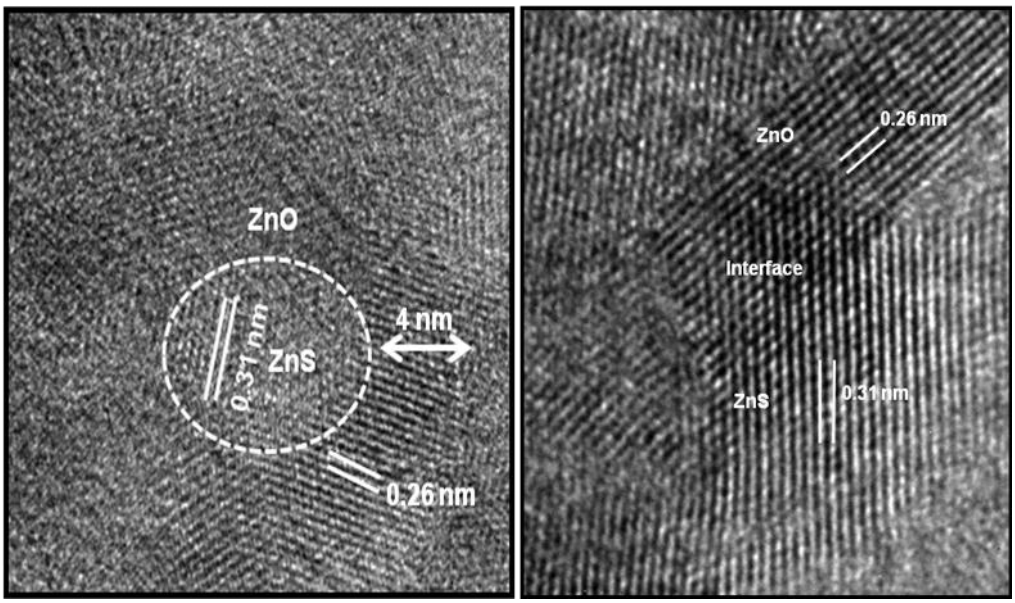

(a) **(b)**

Figure 4.6 HRTEM image of ZnS/ZnO core shell

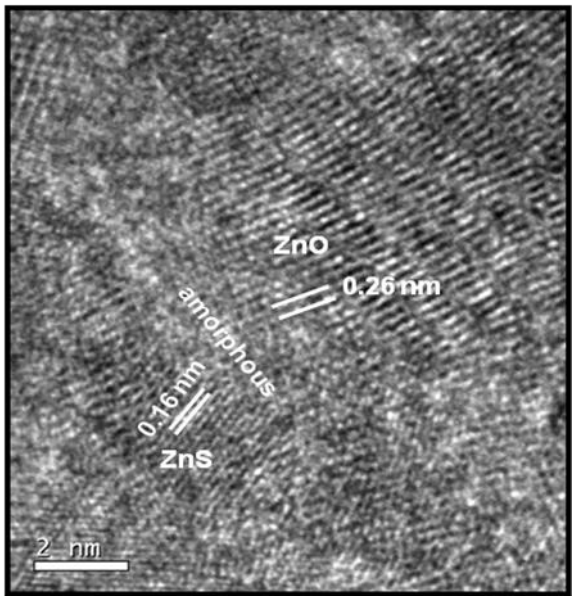

Fig4.6 c

In the HRTEM image as shown in fig 4.5 (a) and (b) with scale bar 20nm and 50 nm the agglomerated particles can be seen. There is also a lighter shaded layer surrounding the darker shaped agglomerate. It is thereby suggested that even before the capping layer starts forming, a few of the ZnS nanoparticles start forming clusters due to their small size related higher dangling bonds at the surfaces. In fig 4.6(a) the clear picture of spherical core and shell can be seen. The d spacing as calculated is 0.31nm that corresponds to (111) plane of Cubic ZnS surrounded by ZnO lattice plane (002) confirmed by the d spacing calculation which is 0.26 nm. The shell thickness is approx. 4nm. There is some overlapping of lattice planes of ZnS and ZnO as can be seen from the fig 6(b). Because of the lattice mismatch there is a development of lattice strain of about 16% in core/shell particles 4.6(a). Higher lattice strain result in an amorphous layer between the planes of ZnS and ZnO as can be seen from fig. 4.6(c).

4.2.4 Optical Properties

Optical Properties of ZnS/ZnO core shell was studied through Photoluminescence Spectra, Time Resolved Spectroscopy and UV-Visible Spectroscopy.

4.2.4.1 Photoluminescence:

4.2.4.1.1 Undoped ZnS Core/ undoped ZnO Shell

PL emission and excitation spectra of ZnS/ZnO core shell particles are shown in Fig.4.7 (a) and (b) respectively.

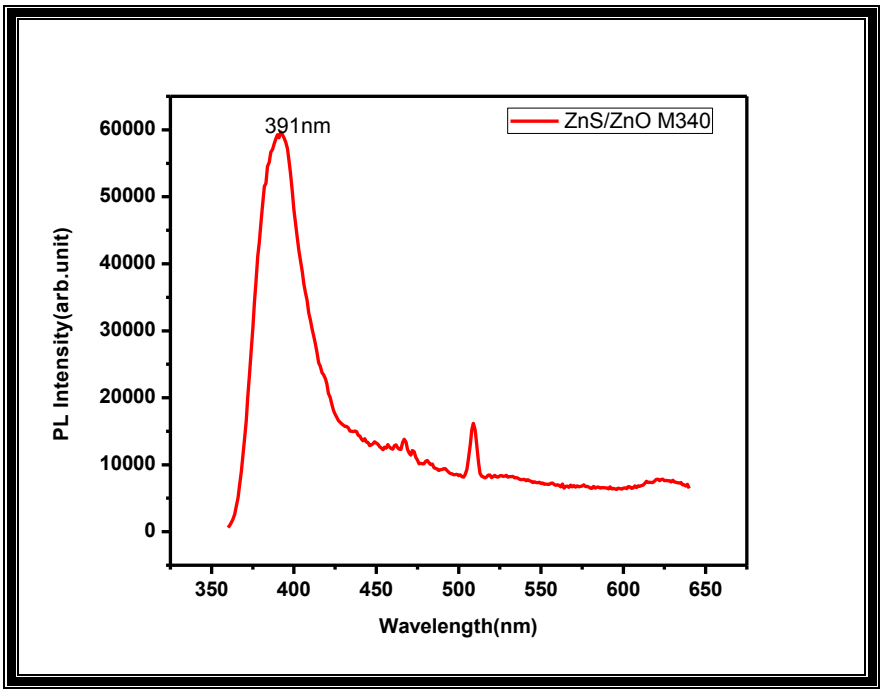

Figure 4.7(a) PL emission Spectra of ZnS/ZnO at excitation of 340nm

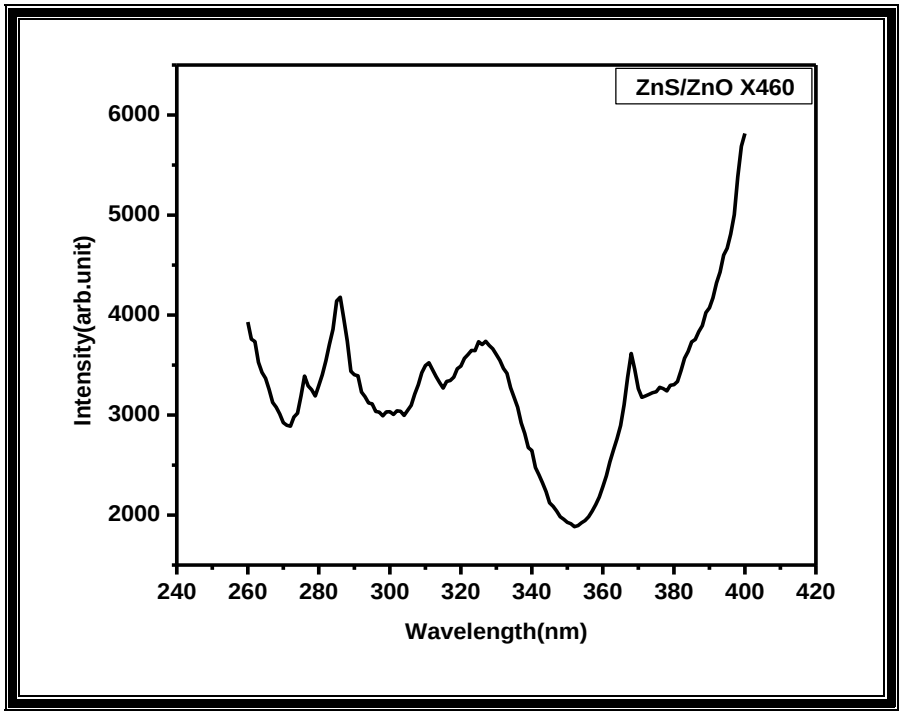

Figure 4.7 (b) PL excitation Spectra of ZnS/ZnO at emission wavelength 460 nm

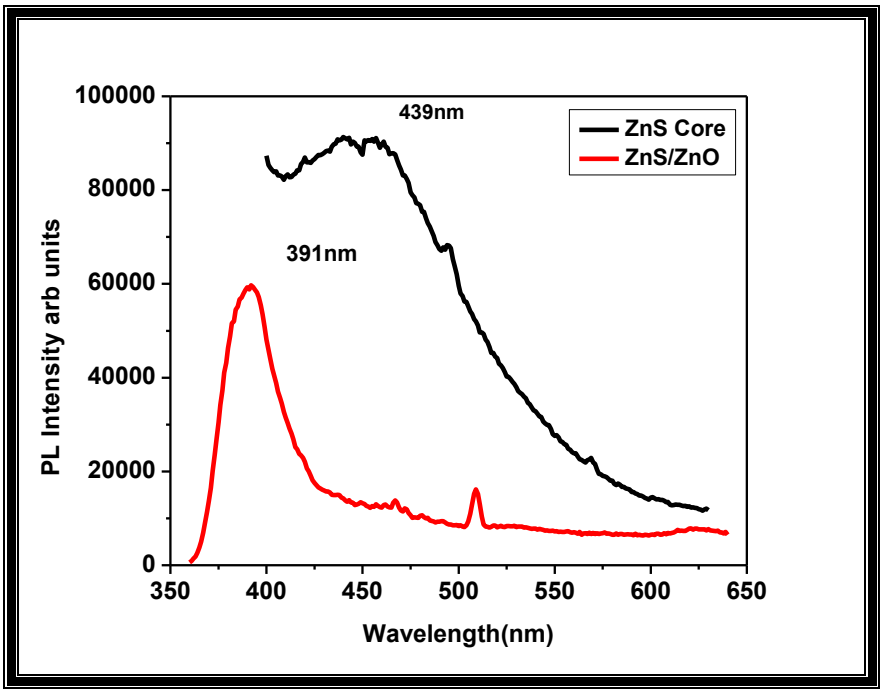

Figure 4.8 PL Emission spectra of ZnS core and ZnS/ZnO core shell nanostructure

The comparison of the PL emission spectra of ZnS core particles and ZnS/ZnO core shell particles are shown in Fig.4.8. The photoluminescence emission spectra of ZnS/ZnO core shell nanostructure shows two emission peaks one at 391nm due to near bandgap excitonic emission of ZnO and another at 440 nm corresponding to ZnS. The figure 8 shows the comparative PL emission curved which shows an additional peak at 391nm along with 440nm peak because of ZnO capping on ZnS there is a drastic decrease in the ZnS emission peak because of the presence of ZnO shell on ZnS core.

4.2.4.1.2 Undoped ZnS Core/ Cr doped ZnO Shell

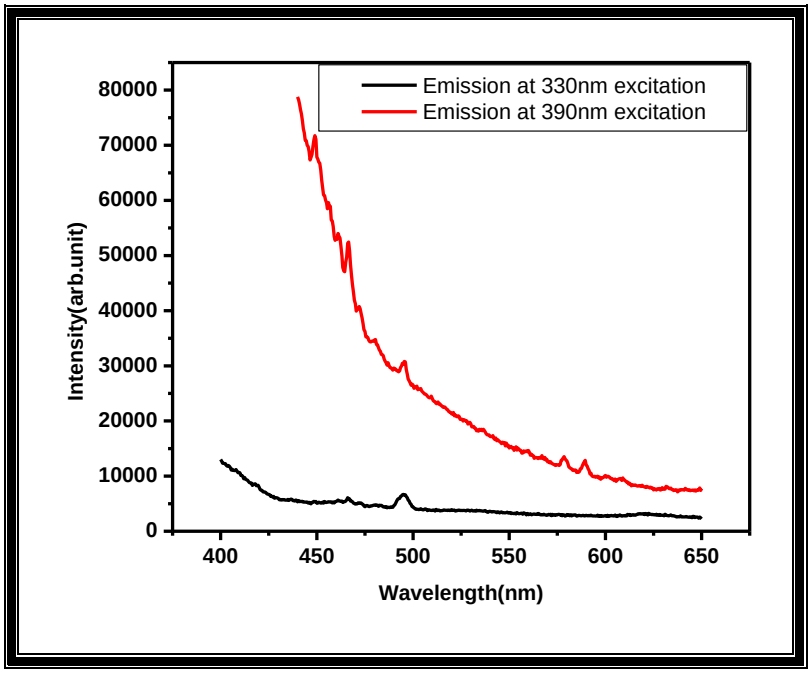

Figure 4.9(a) Emission Spectra of undoped ZnS core with Cr doped ZnO shell excited at 330nm and 390nm

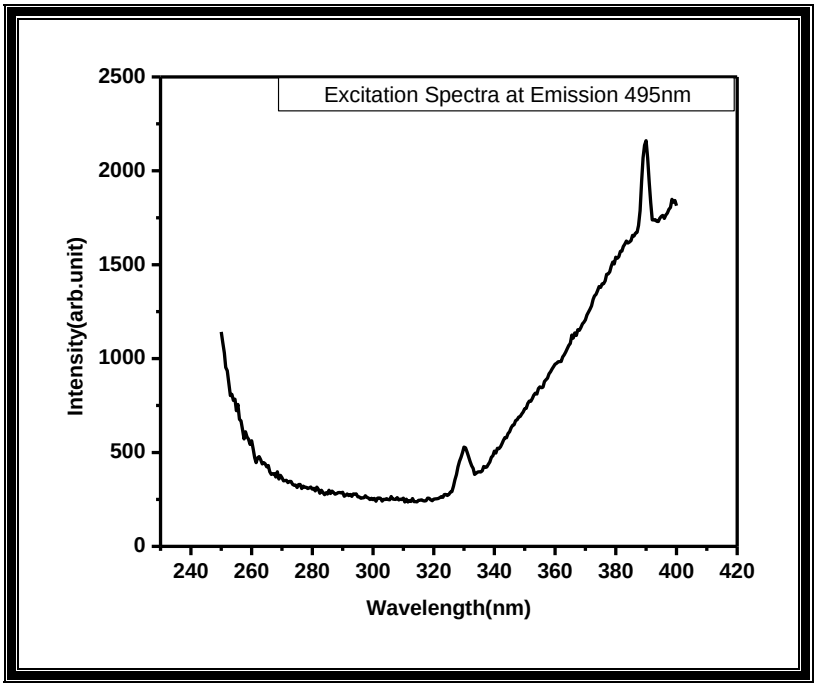

Figure 4.9(b) Excitation Spectra of undoped ZnS core with Cr doped ZnO shell at Emission wavelength 495nm

The Photoluminescence emission curve shown in figure 9a shows an emission of 495nm at the excitation of two wavelength i.e. 330 and 390nm although the peak is of very low intensity that may be because of the chromium doping in the ZnO shell

4.2.4.1.3 Cr doped ZnS Core/ Cr doped ZnO Shell

PL emission and excitation spectra of ZnS:Cr/ZnO:Cr shell is shown in figure 4.10 and 4.11.

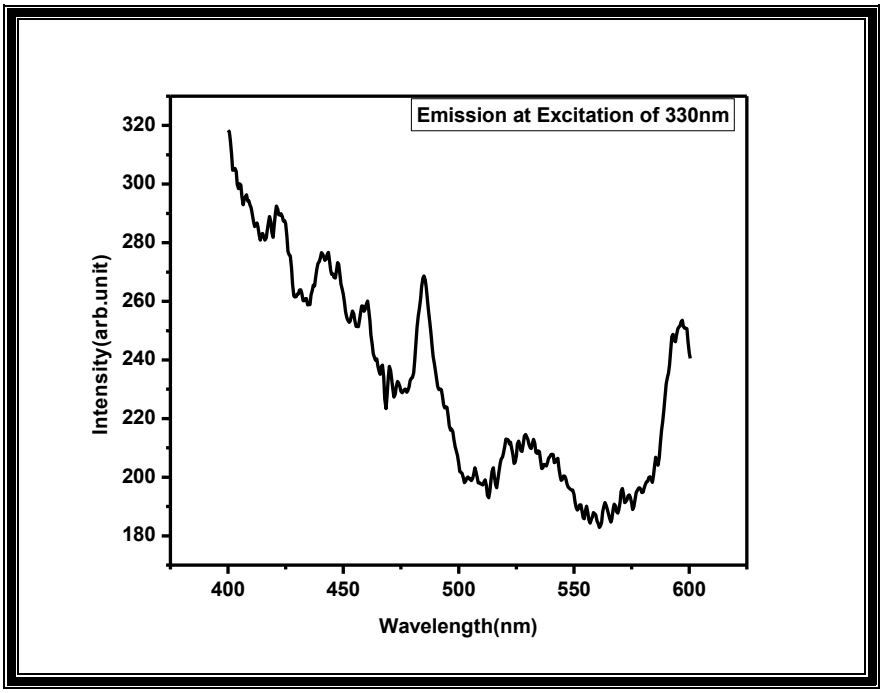

Figure 4.10 (a) Emission Spectra of Doped ZnS core with Doped ZnO shell

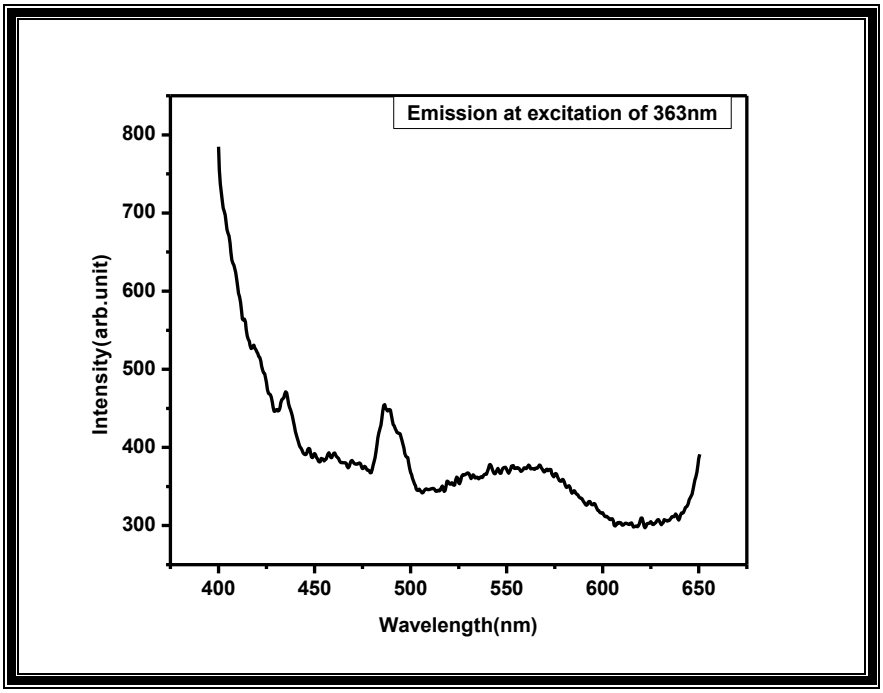

Figure 4.10(b) Emission spectra of Doped ZnS core with Doped ZnO shell Excited at 363nm

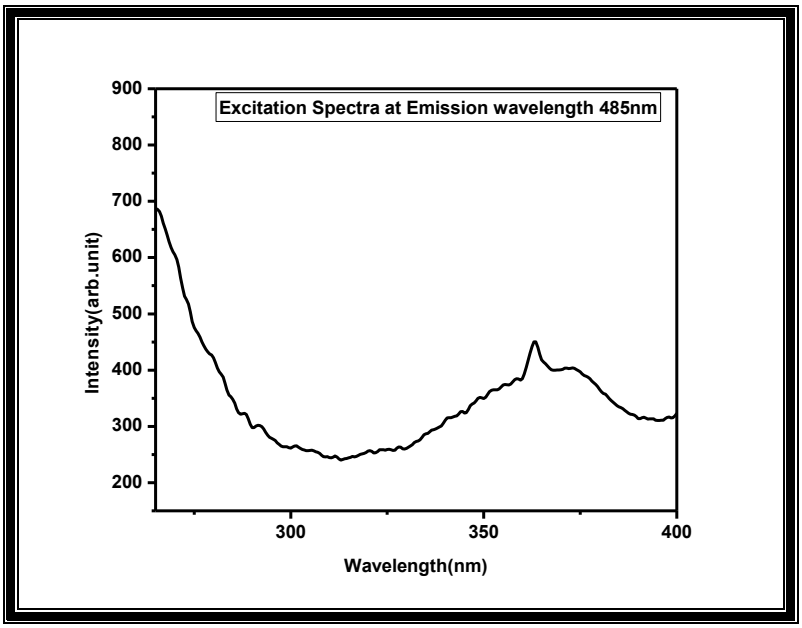

Figure 4.11 Excitation spectra of Doped ZnS core with Doped ZnO Shell at emission wavelength 485nm

PL emission spectra of Cr doped ZnS shell with Cr doped ZnO shell can be seen in fig. 4.10 (a) and (b). There is a sharp emission peak at 485 nm due to the doping of Cr in ZnO shell also sub band emission in the visible region related to the defects or oxygen vacancies in ZnO and produced due to the radiative recombination of a photogenerated hole with an electron occupying the defect or oxygen vacancy. The excitation spectra at an emission wavelength of 485 is given in fig 4.11.

4.2.4.2 Time Resolved Spectroscopy

Decay curve for undoped ZnS core/undoped ZnO shell excited at 330nm wavelength is

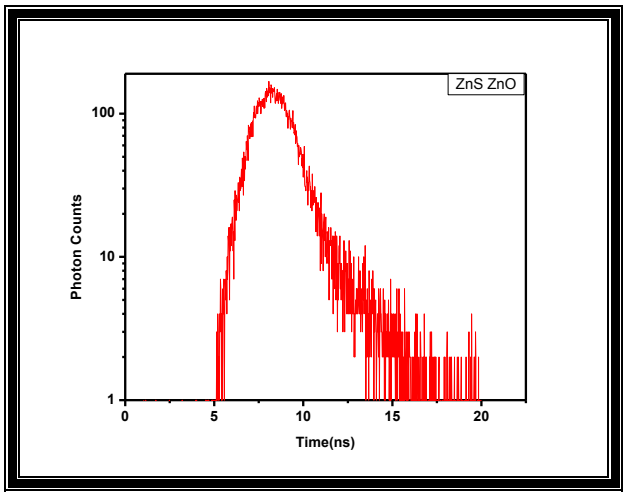

Figure 4.12 (a)decay curve for ZnS/ZnO

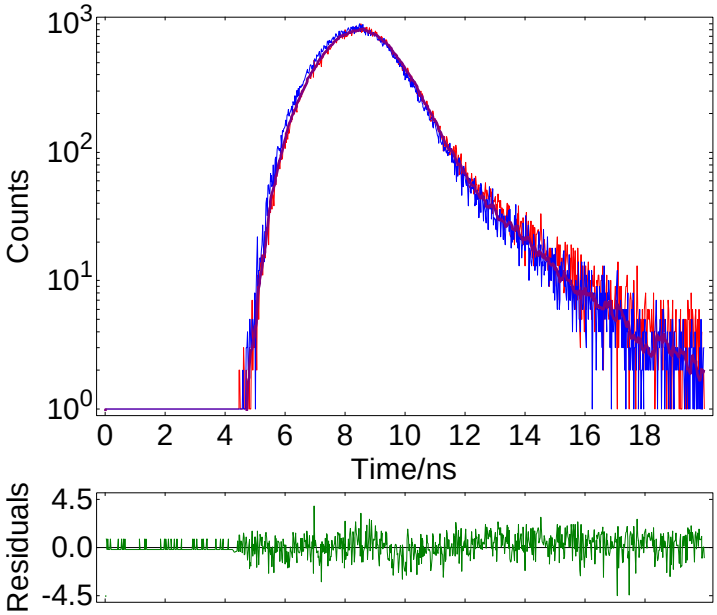

Figure 4.12(b) Linear fit curve for ZnS core with ZnO shell

The linear fit curve of ZnS core and ZnO shell excited at 330 nm and emission at 391nm is given in the fig above. Decay parameters including Characteristic lifetime τ, and pre exponential factor are given in table 1

Decay Parameters

Table 1

τ	1.0263± 0.04068 ns
B1	132.716
A	0.573
χ^2	1.227

The very fast decay time of 1.02 ns comes from the excitonic decay of ZnO 391 nm peak.

Undoped ZnS core with Cr doped ZnO shell

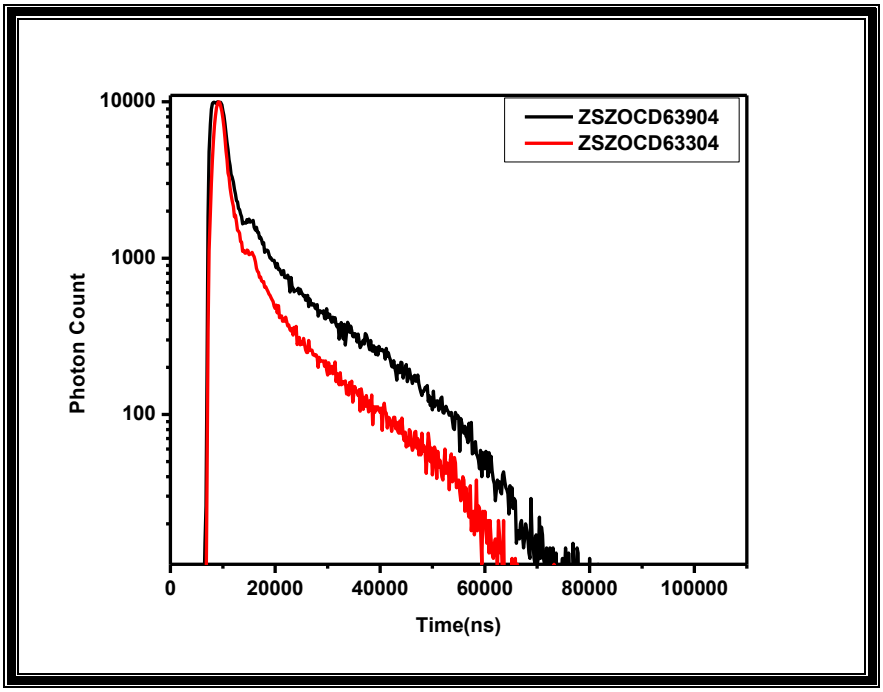

Fig.4.13 Decay curve of ZnS/ZnO:Cr nanoparticles

The decay curve shows a biexponential decay and the parameters for the decay curve for an excitation of 390 nm are listed in table 2

Table 2

Decay Parameters

Lifetime(τ)	microsecond	Relative%
τ_1	0.78	24%
τ_2	6.17	76%

4.2.4.3 UV-Vis Spectroscopy

The absorption and transmission spectra was obtained using UV-Visible spectrometer. The band gap can be directly deduced from the absorption spectra and is verified using the Tauc Plot.

Core Shell

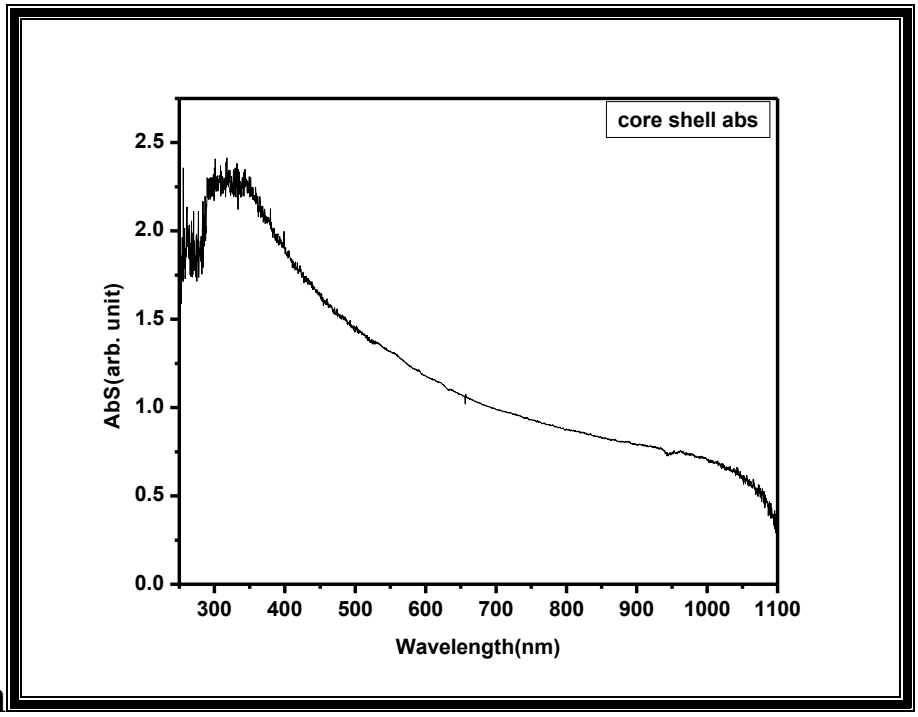

Absorption

Figure 4.14 Absorption Spectra of ZnS/ZnO

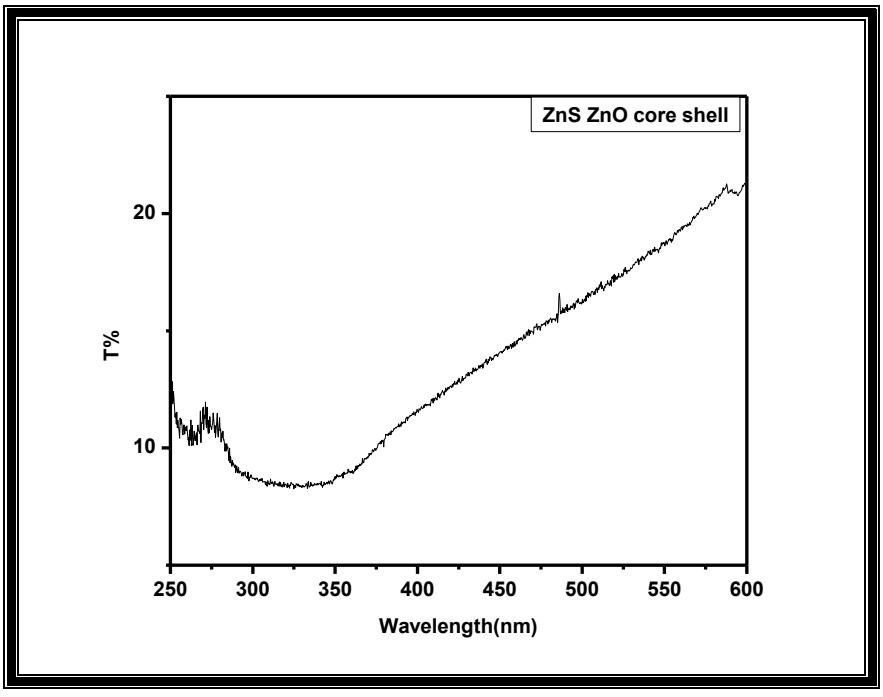

Figure 4.15Transmission Spectra of ZnS/ZnO

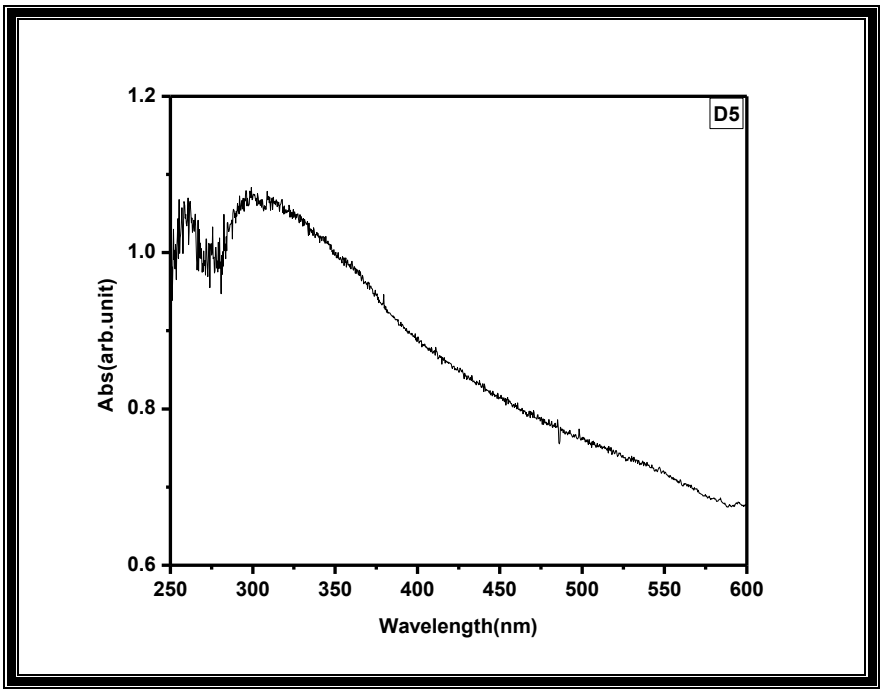

Figure 4.16 Absorption Spectra of Undoped ZnS core with Doped ZnO shell

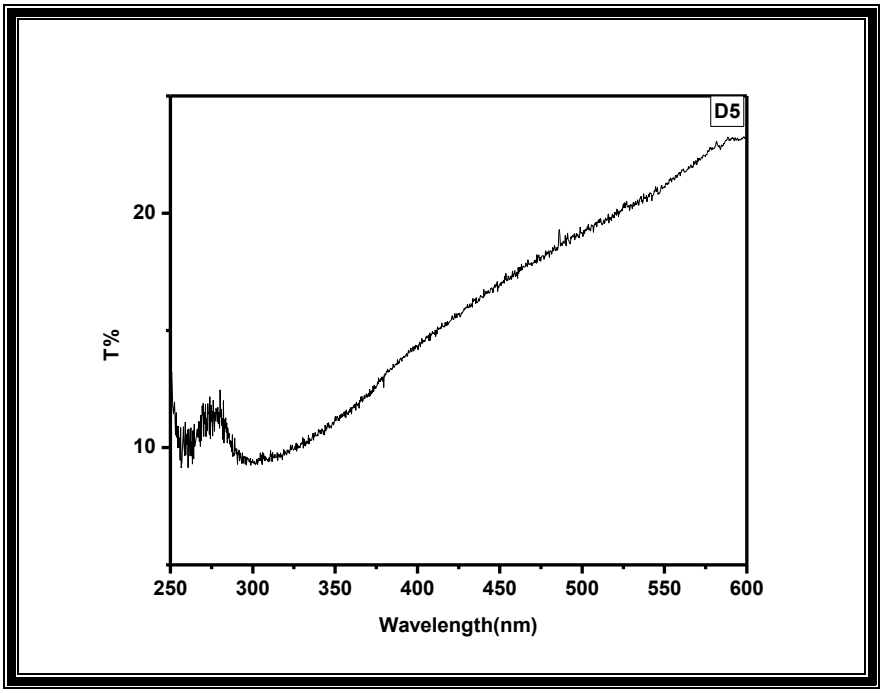

Figure 4.17 Transmission Spectra of Undoped ZnS core with Doped ZnO shell

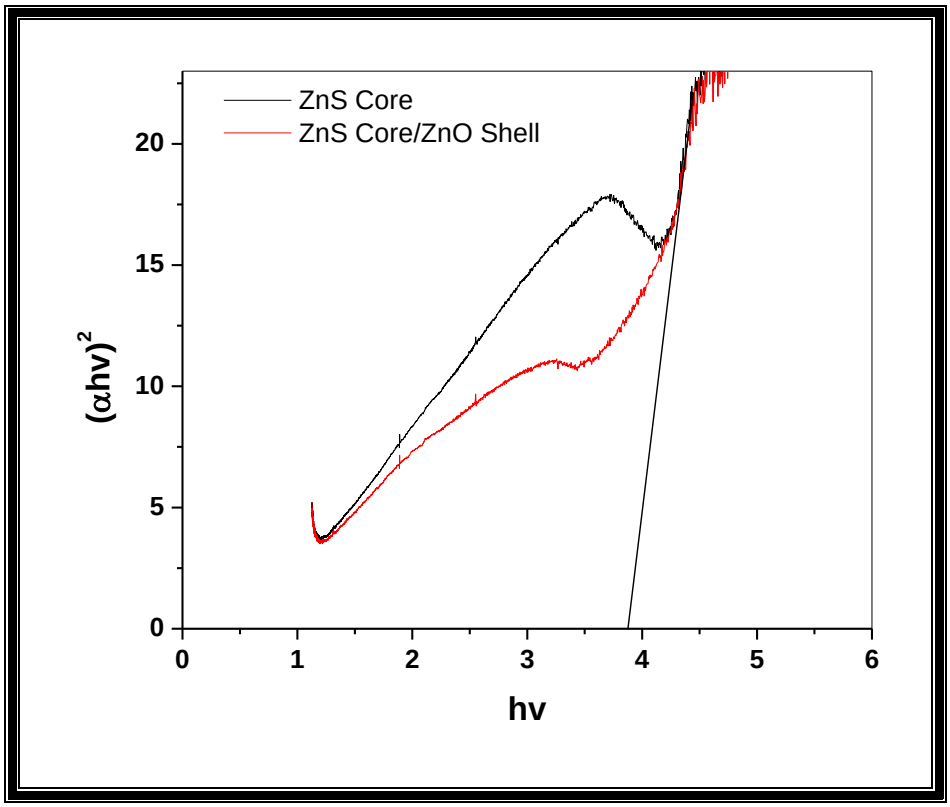

Figure 4.18 Tauc Plot of Zns Core and Zns/ZnO core shell

The absorption spectra of ZnS/ZnO and ZnS/ZnO:Cr in fig 4.15 and fig 4.17 respectively shows a drastic decrease in the absorption intensity. Also there is a slight blue shift in the absorption wavelength. The extrapolation of the linear portion of the Tauc plot of ZnS core and ZnS/ZnO core shell gives band gap of 3.88eV corresponding to ZnS band gap and this matches with the theoretically calculated band gap of ZnS QD with 4 nm diameter as seen in the HRTEM image.

4.2.5 Magnetic Properties

The M-H curves for undoped ZnS core with Cr doped ZnO shell at room temperature and at low temperature (80 K) are shown in fig. 4.20 and 4.21 respectively. The core/shell particles shows paramagnetic behaviour due to ZnO: Cr shell since undoped ZnS core particles are diamagnetic. There is a difference in magnetization value at room temperature and at low temperature with increase in magnetization value at low temperature.

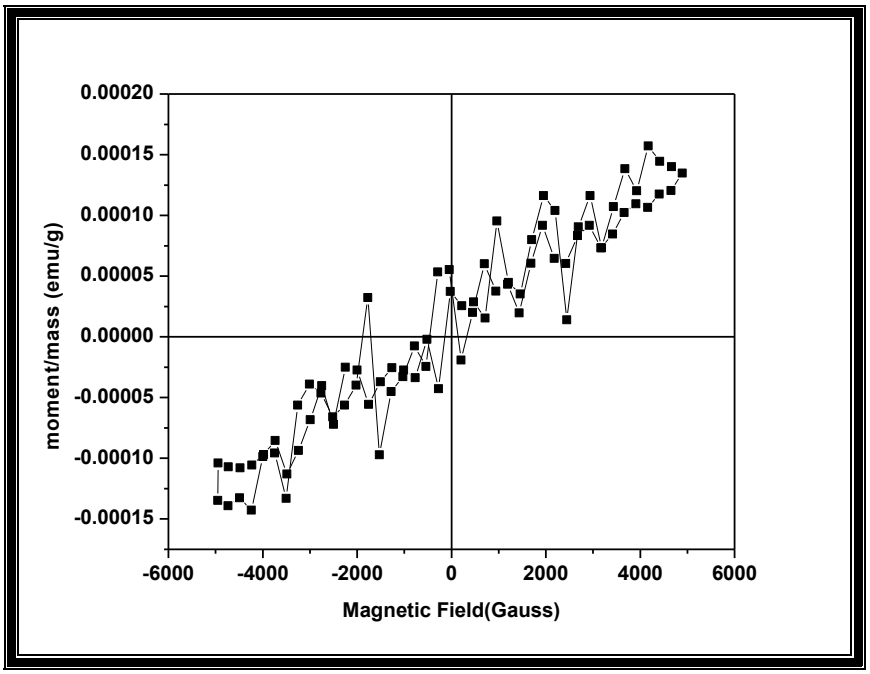

Figure 4.19 M-H curve for undoped ZnS shell with Cr doped ZnO shell at room temperature

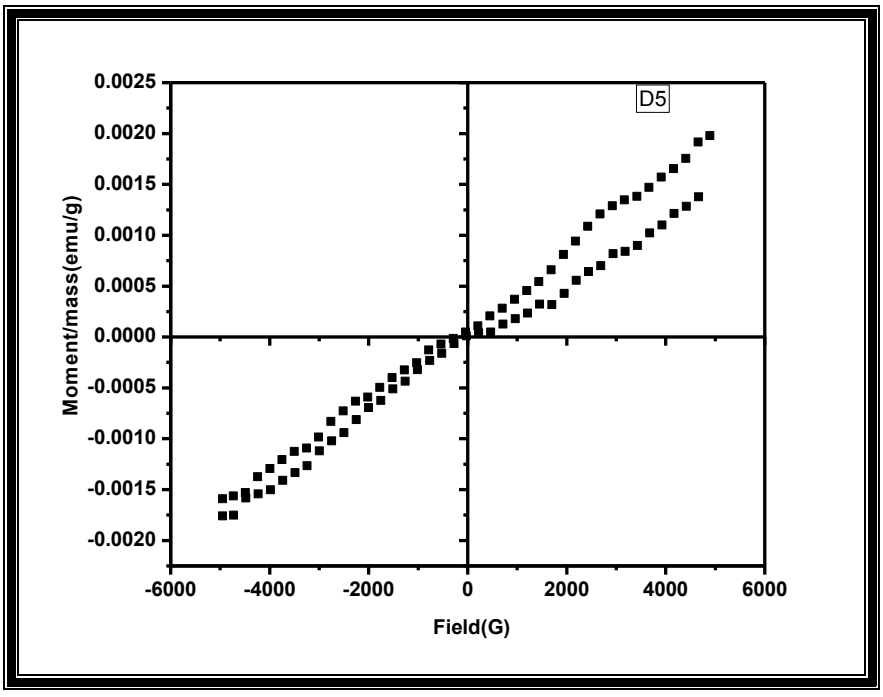

Figure 4.20 M-H curve for Undoped ZnS core with Doped ZnO shell at low temp

4.3 Conclusions

The capping of a lower band gap material on a higher band gap material results in an inverted core shell type of structure. In the present study we were able to successfully cap ZnO on ZnS. The characterization through XRD, TEM and UV- Visible spectroscopy established the as mentioned result. The photoluminescence study for ZnS/ZnO, ZnS/ZnO:Cr and ZnS:Cr/ZnO:Cr suggests that there is a sharp decrease in the luminescence intensity due to the core particle after capping it with ZnO although because of the presence of Chromium in the ZnS core and ZnO shell there is a new peak at 495 nm. The Tauc plot made using the absorption spectra of the core shell nanoparticles gives the two band gap energy one that of ZnS and another of ZnO. The undoped core of ZnS with Cr doped ZnO shell has shown paramagnetic behaviour with the magnetization value greater in case of M-H curve taken at low temperature.

Chapter 5 ZnO/ZnS core shell

We synthesized ZnS/ZnO core shell Quantum dot as explained in chapter 4.The core shell structure thus formed was an inverted core shell with a lattice mismatch giving rise to lattice strain and defect states at the interface acting as trap states for photo generated charge carriers and as a result decreasing the luminescence. This chapter deals with the synthesis of Type I core shell structure by growing a higher band gap ZnS on a lower band gap material ZnO.

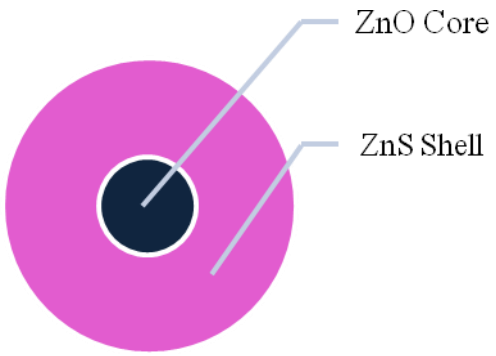

Here we have synthesised ZnO/ ZnS core shell structure by simple wet chemical method.

5.1 Synthesis

Undoped ZnO core with Undoped ZnS shell

Precursors used:

Zinc Acetate	Zinc Chloride
Molecular formula-C_2H_5OOZn	Molecular formula-ZnCl2
Molecular Weight-219.4g	Molecular Weight- 136.14g
Physical State-White Powder	Physical State- Powder
Colour- White	Colour- White
Company- Loba Chemie	Company-Loba Chemie
Sodium Sulphide	**Solvents**
Molecular Formula-Na_2S	Deionized water
Molecular Weight-78.04g	Isopropanol
Physical State- Yellow solid Flakes	
Company- Fine chemicals	

Synthesis Procedure

For Synthesis ZnO/ZnS core shell structure the first step was the synthesis of ZnO core.

Steps for synthesizing ZnO Core
Step1 0.045M of Zinc Acetate solution was prepared in Deionized water
Step2 Double diluted ammonia was added dropwise in order to attain pH 10
Step3 the solution was centrifuged and dried at 90^{o} and was kept in an oven for 24 Hours.

Steps for synthesizing ZnO/ZnS core shell structure are shown below.

ZnO/ZnS core shell
Step 1 0.05 M solution of Zinc Chloride was prepared in Isopropanol
Step2 0.05 M solution of sodium sulphide solution was prepared in isopropanol
Step3 Mix8ml solution A+ 0.1g ZnOcore+2ml Solution B
Step4 The solution was stirred for 30 min
Step5 the resultant mixture was centrifuged and kept in an oven at 90^{0}for 1 hour.

5.2 Result and discussion

5.2.1 Structural Analysis: XRD

The structural analysis of both ZnO core and ZnO/ZnS core shell was done using the XRD.

5.2.1.1ZnO Core

XRD pattern of ZnO core particles is shown in Figure 5.1 conforming to hexagonal wurtzite structure.

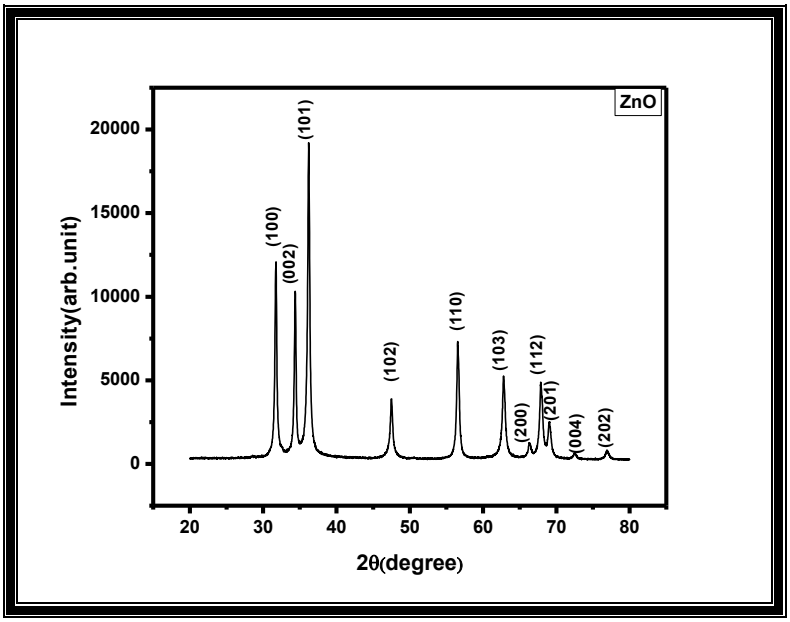

Figure 5.1 XRD pattern of ZnO particles synthesised using aqueous chemical method

The XRD pattern of ZnO core shows sharp peaks at 31.7°,34.3°,36.3°,47.3°,56.4°,62.8°,66.2°,67.8°,69.0°,72.5° and 76.9° which corresponds to (100),(002),(101),(102),(110),(103),(200),(112),(201),(004) and (202) planes of hexagonal structure of ZnO verified from the standard data i.e. JCPDS card no. 89-1397. The particle size as calculated from the peak at 36.22° using Debye Scherrer formula is 46.3 nm.

5.2.1.2ZnO core/ZnS shell

The XRD pattern of the ZnO core/ZnS shell particles is shown in Fig.5.2.

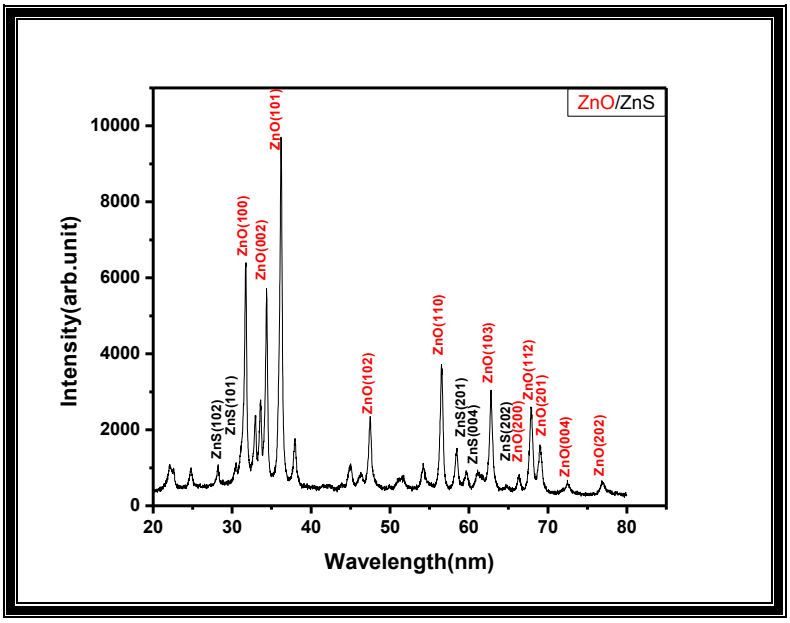

Figure 5.2 XRD pattern of ZnO core and ZnS shell structure

From fig. 5.2 the XRD pattern of ZnO/ ZnS core shell can be seen where along with the major peaks of ZnO there are peaks at 28.1°,30.5°,58.3°,59.6° and 64.8° corresponding to (102),(101),(201),(004) and (202) planes of hexagonal ZnS structure as confirmed from the JCPDS card no (30-0007). This confirms the epitaxial growth of ZnS hexagonal structure on hexagonal ZnO. Some extra peaks can be seen in fig 2. which may be due to residual precursors zinc chloride and Sodium sulphide.

5.2.2 Morphological study

The morphological studies of the as prepared samples were done through SEM. The fig 5.3 (a)-(d) shows the SEM images with different magnification of ZnO/ZnS core shell structure. SEM micrographs show very small particles as well as sheet type structure.

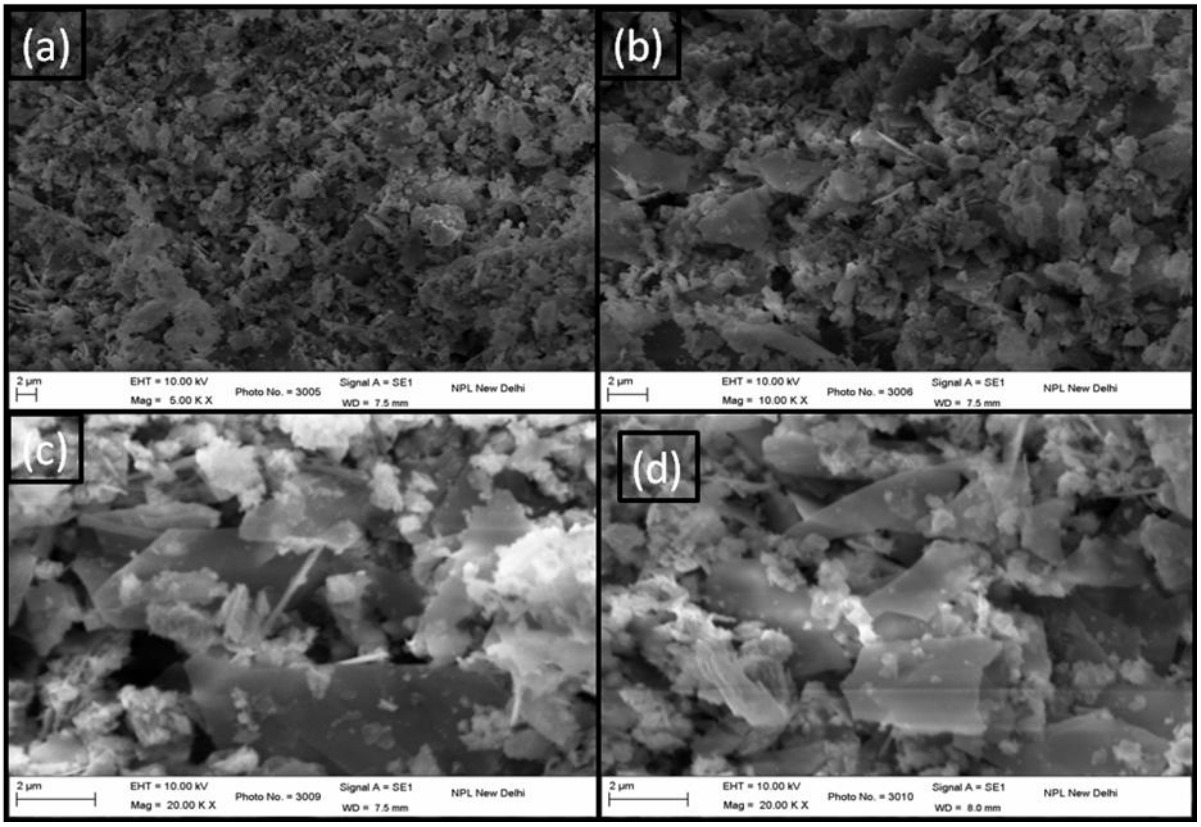

Figure 5.3 SEM images of ZnO/ZnS core shell structure at different magnifications

5.2.3 Optical Properties

Study of the optical properties is done through Photoluminescence emission and excitation spectra.

Photoluminescence

The PL excitation and emission spectra of ZnO core particles and ZnO core/ZnS shell particles have been measured and compared. The Pl emission spectra have been measured at two excitation wavelengths namely 218 nm and 340 nm. Fig 4 and 5 exhibits the PL emission spectra of core and core shell particles at 218 nm and 340 nm respectively. PL excitation spectra at 389 nm is shown in fig.5.6

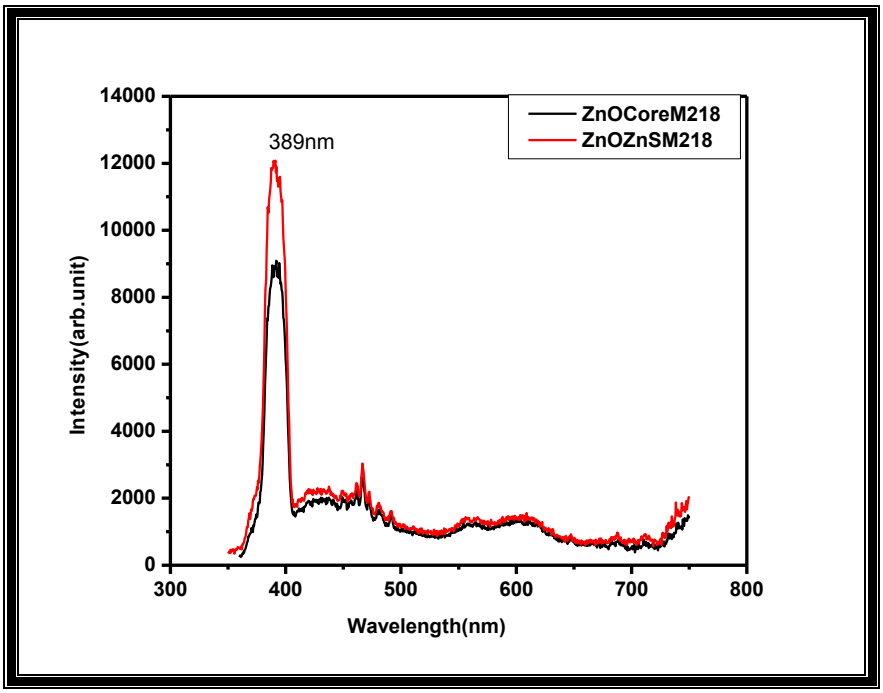

Figure 5.4 PL emission spectra of ZnO core and ZnO/ZnS core shell at an excitation of 218 nm

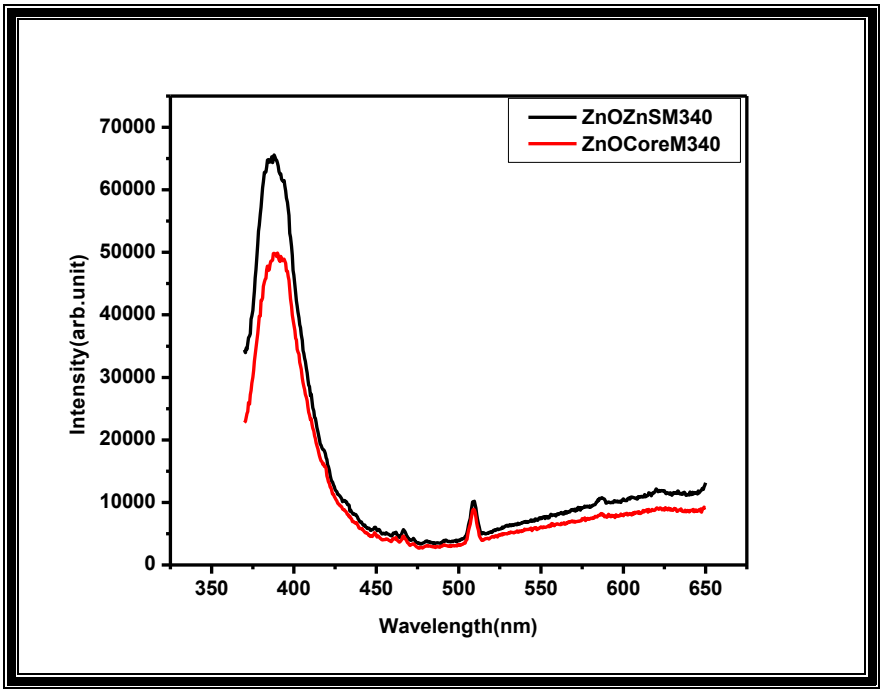

Figure 5.5 PL emission Spectra of ZnO and ZnO/ZnS core shell at an excitation wavelength of 340 nm

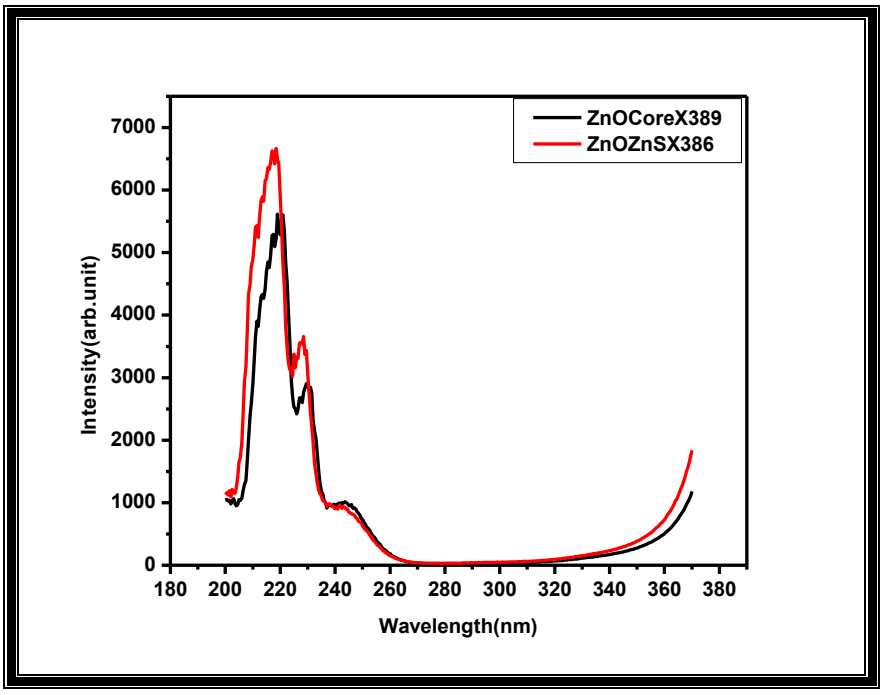

Figure 5.6 PL excitation Spectra of ZnO and ZnO/ZnS core shell at an emission wavelength of 389 nm

The sharp peak at 389nm is because of near band edge excitonic emission of ZnO core particles due to free exciton recombination. Visible emission of much lesser intensity is also present which may be because of intrinsic defects such as oxygen and zinc interstitials. The emission for ZnO/ZnS is also plotted in the same graph for comparison and the enhanced photoluminescence intensity at 389nm is clearly visible and is attributed to the capping of a higher band gap material that is ZnS on the lower band gap ZnO. Hence in a core shell structure of lower band gap core material surrounded by a higher band gap shell material, enhancement of photoluminescence emission is clearly observed.

Conclusions

ZnO / ZnS core shell structure was formed at room temperature by a wet chemical process. The XRD shows the formation of ZnS as well as ZnO in hexagonal phase as matched with standard data of JCPDS and the size of core particle calculated using scherrer formula is about 46 nm which is quite small. The morphological study through SEM shows formation of some sheets like structure. The core ZnO and shell ZnS both have hexagonal structure hence there is no lattice mismatch its effect can be seen in the PL spectra. The core shell structure is a normal type I structure as can be predicted from the PL spectra a there is an enhancement in Photoluminescent emission intensity.

References

[1] Jonghyun Park and Wei Lu, Applied Physics Letters 91, 053113 ,2007

[2] D. Battaglia, J. J. Li, Y. J. Wang, X. G. Peng, Angew. Chem. Int. Ed. 42, 5035–5039,2003

[3] X. H. Zhong, R. G. Xie, Y. Zhang, T. Basche´, W. Knoll, Chem. Mater. 17, 4038–4042,2005

[4] D. Battaglia, J. J. Li, Y. J. Wang, X. G. Peng, Angew. Chem. Int. Ed. 42, 5035–5039, 2003

[5] P. Sarkar, M. Springborg, G. Seifert, Chem. Phys. Lett., 405, 103–107, 2005

[6] J. B. Li, L. W. Wang, Appl. Phys. Lett. 84, 3648–3650,2004

[7] Piryatinski, S. A. Ivanov, S. Tretiak, V. I. Klimov, Nano Lett., 7, 108–115,2007

[8] Peter Reiss,* Myriam Protie`re, and Liang Li, Small.,154-68,2009

[9] X. X. He, K. M. Wang, W. H Tan, et al, J. Nanosci. Nanotech., 2,3,217-230,2009

[10] X. X. He, J. H. Duan, K. M. Wang, et al, J.Nanosci. Nanotech., 4,1-5,2003

[11] Y. Yuan, X. X. He, K. M. Wang, et al, Chemical Journal of Chinese Universities, 3,446-448,2005

[12] Marvin C. Goldberg and Eugene R. Weiner U.S. Geological Survey, Box 25046, MS 424, Lakewood, CO 80225

[13] Kemin Wang*, Weihong Tan, Xiaoxiao He, Proceedings of the 2005 IEEE Engineering in Medicine and Biology 27th Annual Conference Shanghai, China, September 1-4, 2005

[14] C. A. Leatherdale, W.-K. Woo, F. V. Mikulec, and M. G. Bawendi - On the Absorption Cross Section of CdSe Nanocrystal Quantum Dots - J. Phys. Chem. B, 106 (31), pp 7619–7622,2002

[15] Demir Akin, Jennifer Sturgis, Kathy Ragheb, Debby Sherman, Kristin Burkholder, J. Paul. Robinson, Arun K. Bhunia, Sulma Mohammed & Rashid Bashir, Nature Nanotechnology, 2, 441,2006

[16] Development of nanophosphors – a review, Mater. Sci. Engin. R 49 (2005), pp. 113–155

[17] R. Menner, B. Dimmler, R.H. Mauch and H.W. Schock, J. Cryst. Growth 86 p. 906,1998

[18] M. Jayalakshmi[a] and M. Mohan Rao Journal of Power Sources Volume 157, Issue 1, Pages 624-629,19 June 2006

[19] http://epswww.unm.edu/xrd/xrdclass/01-XRD-Intro.pdf

[20] http://serc.carleton.edu/research_education/geochemsheets/techniques/XRD.html

[21] http://serc.carleton.edu/research_education/geochemsheets/techniques/SEM.html

[22] http://nobelprize.org/educational/physics/microscopes/tem/index.html

[23] http://inventors.about.com/od/pstartinventions/a/Photoluminescen.htm

[24] http://cnx.org/content/m34525/latest/

[25] http://uweb.txstate.edu/~ab35/manuals/VSM/vsm.pdf

[26] J.Tauc,Amorphous and liquid semiconductors,J.Tauc Edi,New York,Plenum,(1974)
[27] Harish Chander and Santa Chawla Bull. Mater. Sci., Vol. 31, No. 3, pp. 401–407 June 2008,